JOURNAL OF GEOPHYSICAL RESEARCH, VOL. 114, D06213, doi:10.1029/2008JD010679, 2009

Impact of Arabian Sea pollution on the Bay of Bengal winter monsoon rains

T. N. Krishnamurti,[1] Arindam Chakraborty,[1] Andrew Martin,[1] William K. Lau,[2] Kyu-Myong Kim,[3] Yogesh Sud,[2] and Gregory Walker[4]

Received 29 June 2008; revised 8 October 2008; accepted 12 January 2009; published 28 March 2009.

[1] Accumulation of pollution over the southern Arabian Sea has been documented in numerous studies that followed the INDOEX field project of 1992. In this paper, we show several examples of this feature from the MODIS/CALIPSO data sets. We identify this feature as the Bombay Plume that makes its way into the Arabian Sea from the west coast of India. A second part of this work is on modeling the impacts of pollution. We use a NASA Goddard Earth Observing System (GEOS) model to carry out many comparative forecast simulation experiments that include the pollution based on MODIS and control runs that utilize climatological estimates of pollutions. The model invokes both the direct and indirect effects of aerosols. Our observations are as follows: (1) The Arabian Sea experienced above normal rain during these periods for the MODIS experiments as compared to the control. (2) The most interesting feature is the divergent outflow center, in the upper troposphere, over polluted regions of the atmosphere over the Arabian Sea as a consequence of tropospheric aerosol heating. (3) An important related feature is a compensating downward lobe with a divergent inflow in the upper troposphere center over the Bay of Bengal. (4) The presence of this downward lobe over the Bay of Bengal relates to a reduction of winter monsoon rains over the southeast coast of India. (5) We also show evidence of similarly reduced winter monsoon rains in raingauge data over the southeast coast of India during high-pollution events ascertained from MODIS data.

Citation: Krishnamurti, T. N., A. Chakraborty, A. Martin, W. K. Lau, K.-M. Kim, Y. Sud, and G. Walker (2009), Impact of Arabian Sea pollution on the Bay of Bengal winter monsoon rains, *J. Geophys. Res.*, *114*, D06213, doi:10.1029/2008JD010679.

1. Introduction

[2] Recently there have been major concerns about the source of anthropogenic aerosols over the Asian regions and the resulting impact on the monsoon circulation and rainfall as well as air quality and health [*Ramanathan et al.*, 2001a, 2005]. Industrial development and biomass burning in South and East Asian countries are the major source of these pollutants. Satellite observations show that these aerosols cover the region from most of China to the foothills of the Himalayas and to the south of Arabian Sea. These were named as ABC [*Ramanathan et al.*, 2001b; *Ramanathan and Crutzen*, 2003] and are most prominent during the postsummer monsoon to the presummer monsoon seasons (October–April; a list of acronyms is provided in Table 1). The scavenging by convective clouds and precipitation washes down the aerosols during the summer monsoon season.

[3] Recent studies of *Ramanathan and Ramana* [2005] and *Lau et al.* [2006, 2008] has placed a strong emphasis on the possible effects of aerosols and dust on the behavior of the monsoon. *Lau et al.* [2006] examined the sequential effects of aerosols as they impacted an entire monsoon season. They suggested that atmospheric heating by absorbing aerosols would result in water cycle feedbacks and strengthen the south Asia monsoon. Our study essentially addresses such monsoon impacts from a model sensitivity point of view, where we compare the precipitation impacts due to the presence or absence of the direct and indirect effects of aerosols on the short-wave and long-wave radiative transfers. We also examine regional teleconnections via regional anomalies.

[4] The anthropogenic aerosols also modulate the radiative forcing [*Satheesh and Ramanathan*, 2000] by absorbing short-wave radiation in the lower troposphere (heating effect) and thereby reducing the amount of radiation reaching the ground (cooling effect). These are called first and second direct effects. Aerosols also impact the hydrological

[1]Department of Meteorology, Florida State University, Tallahassee, Florida, USA.
[2]Laboratory for the Atmospheres, NASA Goddard Space Flight Center, Greenbelt, Maryland, USA.
[3]Goddard Earth Sciences and Technology Center, University of Maryland, Baltimore County, Baltimore, Maryland, USA.
[4]Science Applications International Corporation, Beltsville, Maryland, USA.

0148-0227/09/2008JD010679$09.00

Table 1. List of Acronyms Used in This Study

ABC	Atmospheric Brown Cloud
ADE	Aerosol Direct Effect
AGCM	Atmospheric General Circulation Model
AIE	Aerosol Indirect Effect
AOD	Aerosol Optical Depth
BP	Bombay Plume
CALIPSO	Cloud-Aerosol Lidar and Infrared Pathfinder Satellite Observation
CCN	Cloud Condensation Nuclei
CER	Cloud Effective Radius
CLW	Cloud Liquid Water
COD	Cloud Optical Depth
DJF	December-January-February
EAS	Eastern Arabian Sea
EOS	Earth Observing System
GEOS	Goddard Earth Observing System
GOCART	Georgia Institute of Technology-Goddard Global Ozone Chemistry Aerosol Radiation and Transport
GSFC	Goddard Space Flight Center
HDF	Hierarchical Data Format
INDOEX	Indian Ocean Experiment
LIDAR	Light Detection and Ranging
MODIS	Moderate Resolution Imaging Spectroradiometer
NASA	National Aeronautics and Space Administration
NCAR	National Center for Atmospheric Research
NCEP	National Center for Environmental Predictions
PDF	Probability Distribution Functions
SST	Sea Surface Temperature
TMI	TRMM Microwave Imager
TRMM	Tropical Rainfall Measurement Mission

cycle by impacting the cloud microphysics [*Satheesh et al.*, 2002; *Menon et al.*, 2002]. First, they increase the number of cloud drops and second the smaller drops take longer to become precipitating hydrometeors through precipitation microphysics. These are called first and second aerosol indirect effects.

[5] The western Indian cities of Mumbai and Pune exhibit a high concentration of technology/heavy industry [*Gradel and Crutzen*, 1993]. These cities are a source of anthropogenic aerosols such as CO and VOC's (black carbons) as well as NO_x and O_3 [*Phadnis et al.*, 2002]. In previous studies, transport of black carbon-rich air from Western/Northwestern India over the Arabian Sea has been described as the ''Bombay Plume'' [*Lobert and Harris*, 2002; *Lelieveld et al.*, 2001]. While the phenomenon has been identified, the atmospheric conditions that lead to BP, its vertical structure, and its effects on physical parameters over the oceans are unclear. This study will identify cases of high aerosol loading over the EAS near the cities of Mumbai/Pune, India using the MODIS instrument data aboard NASA's Terra/Aqua satellites. We will identify the atmospheric conditions/flow regimes that contribute to the BP using the NCEP reanalysis wind data. The vertical structure/extent of the BP using the 1064 nm LIDAR backscatter detector on board NASA's CALIPSO satellite is also examined. The study also invokes the effect of BP aerosols on cloud hydrometeor properties over the EAS with PDF's derived from MODIS and observations from NASA's TRMM. This paper will discuss the nature of the Bombay Plume and its effect on atmospheric conditions over the nearby ocean as the first step in a verification of forecasts from the GEOS-4 Atmospheric General Circulation Model developed by NASA-GSFC. Modeling of the effects of absorbing aerosols on the winter monsoon rains is addressed later in this paper.

2. Observational Aspects

[6] MODIS, CALIPSO and TRMM satellite remote sensing instruments, as well as NCEP's daily global reanalysis products provide observational data for this study. MODIS provides the primary data source for resolving the BP and tracking it across the EAS. MODIS consists of a 36-channel spectroradiometer. Nine channels of approximately a 20-nm bandwidth in the infrared spectral region are used to resolve aerosol properties. Additional eight channels covering more bandwidth in the higher wavelengths (near infrared and visible) are used to resolve cloud properties. The MODIS spectroradiometer is carried on two EOS satellites: Terra and Aqua. Terra makes descending polar orbiting passes over the tropic of cancer near 10:30 local time. Likewise, Aqua passes in ascending orbit near 13:30 local time. The MODIS atmosphere group uses algorithms to create a combined land-ocean mean total aerosol optical depth (AOD; at 0.55 μm), aerosol mean particle size, and fine particulate (radius <0.5 μm) to coarse particulate (radius >1.0 μm) ratio [*Hubanks*, 2007]. In addition, spectral radiance and cloud mask grids observed by MODIS are used to calculate several cloud optical properties for grid squares in which clouds are present. Through lookup table algorithms, MODIS data retrievals provide cloud optical thickness and effective cloud drop radius. MODIS data has spatial resolution of 0.5 km for the aerosol resolving channels, and 1 km for cloud product channels [*Hubanks*, 2007]; however, the data is regridded to 1° latitude resolution in the HDF archive. MODIS can resolve AOD over oceans and dark vegetated land surfaces, but is unable to retrieve the data over deserts or ice. In addition, the length resolved transverse to the orbital path (footprint) from consecutive passes does not overlap [*Lorentz*, 2007]. Thus the daily data from each satellite contains gaps, which hinders resolving the entire BP on any given day. Because the BP is a local feature on a small spatial and temporal scale, (only over the EAS for 3–7 days) we combined the AOD grids from both Terra and Aqua to create our principal data set. We use the arithmetic mean of AOD over the grid cells for which Terra and Aqua data overlapped.

[7] Data from CALIPSO provided information about the vertical extent and structure of the BP. CALIPSO carries a LIDAR instrument (CALIOP) that measures backscatter from aerosols and cloud droplets in the visible light range. The satellite follows the same orbit as the MODIS Aqua satellite, lagging by about 2 minutes. The LIDAR instrument on CALIPSO is capable of measuring aerosol vertical profiles, and AOD. Unlike MODIS, CALIPSO's footprint has very small width and is only suited for vertical profiling of aerosols, but not the horizontal distribution. Vertical extent and distribution of relative backscatter radiances in an aerosol features can be retrieved directly from the CALIPSO website in the form of vertical cross-section images. A mix of MODIS and CALIPSO data provides the vertical structure of aerosols.

[8] Data sets from the TRMM were needed for examining the interaction between aerosols of the BP and hydrometeors and SST over the EAS. TRMM contains many

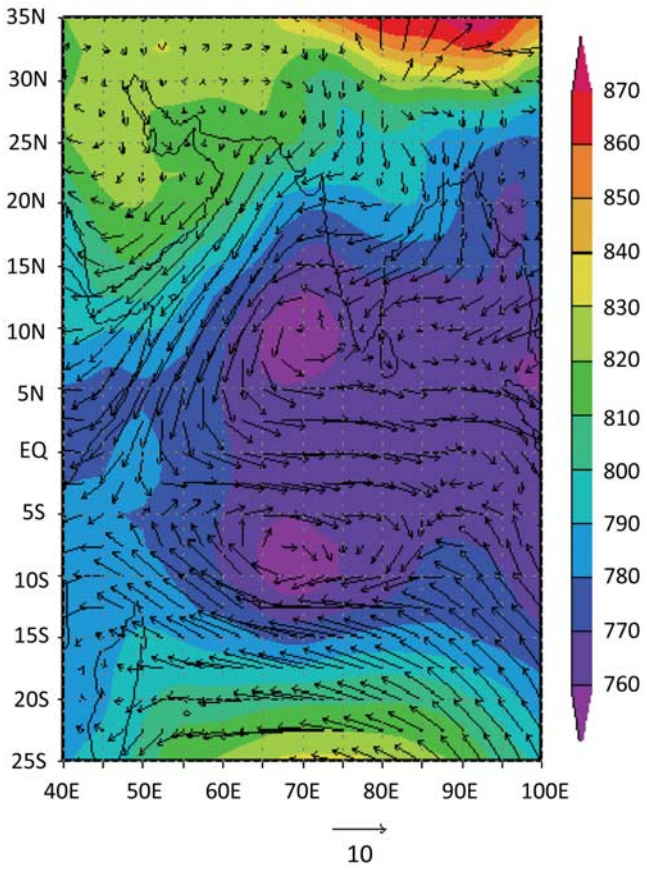

Figure 1. Composite of 925-mb winds and geopotential heights for all Bombay plume events on 2003–2007 during DJF.

instrument packages focused on tropical hydrology. The TMI provided SST and CLW grids. TMI is a passive microwave sensor. Over the ocean, TMI resolves atmospheric water by its emission curve with the help of the cold background dimming property of large bodies of water [*Adler*, 2006]. Large bodies of water appear dimmer in the microwave region than Planck's law predicts, but microwave emission from water (liquid and vapor) suspended in the atmosphere largely follows its predicted Planck curve [*Adler*, 2006]. Thus TMI only takes measurement over the oceans. The TRMM satellite has a low inclination orbit, which only takes it between 35°N and 35°S latitude [*Simpson et al.*, 1988]. As with Terra/Aqua, it takes several passes for complete global coverage from TRMM. In addition, the TRMM data sets provided rainfall estimates, especially over oceans, for this study.

2.1. Plume Transport

[9] Our study focused on the observational and modeling aspects of the direct and indirect effects of aerosols. Mumbai is located on the Middle Western coast of India on the EAS. *Krishnamurti et al.* [1997] have identified the dominant flow in the region at low levels as northeasterly during winter monsoon months. This should tend to transport aerosols created in Mumbai and Pune out to sea and to the southwest. Accordingly, the task was to identify Mumbai/Pune as the source region of these particles. To this end, a case list was compiled of "typical" Bombay Plume events during DJF from 2003 to 2007. This period was chosen because AOD data was available from both Terra and Aqua satellites. A typical event satisfied two criteria. First, the AOD exceeded 0.35 for an area average between 67 to 72E longitude and 13 to 18N latitude. Second, winds had to be northeasterly for 3 or more days surrounding peak AOD. The AOD threshold was chosen based on observations of MODIS AOD over the Arabian Sea during the winter season, while the wind criterion was chosen to ensure that the Bombay area was a possible source of the aerosols in the plume. From this case list, two attributes of the Bombay Plume were apparent. A typical winter monsoon plume event lasts around 5 days. Furthermore, the low-level flow that drives a typical event is caused by an Arabian Sea surface high pressure system, in conjunction with low pressure at the surface near the Maldives. These features are seen in the composite of winds and 925 hPa heights from the case list, as illustrated in Figure 1.

[10] A composite of average AOD and 925 hPa winds was made from the case list by averaging the parameters (horizontal winds, AOD) over all cases during the central event day, 1 day prior, 2 days prior, 1 day after, and 2 days after the event. This was done for total AOD. The day-by-day perturbation composite is shown in Figure 2. Values in the perturbation correspond to the total AOD composite with the 5-day mean subtracted. The composites show that the BP originates in West Central India near Mumbai and Pune 2 days prior to the highest AOD concentrations over the EAS. A typical Bombay Plume may take a northward turn toward the Gulf of Cambay before being caught in a low-level jet (see Figure 1) which speeds transport to the southwest.

2.2. Vertical Extent

[11] CALIPSO has been in operation only since mid-June of 2006. Only three cases of "typical" DJF Bombay Plumes occurred in the intervening period. CALIPSO was overhead on a relatively clear day for two of these. CALIPSO's visible light backscattering requires clear sky condition in the middle and upper levels for resolving the Bombay Plume. The CALIPSO instrument can only discern through very thin clouds. Good images of the BP exist for 5 December 2006 and 9 and 11 January 2007. Figures 3a and 3b show that The Bombay Plume exists only below 3 km, and is even lower when further away from the continent. This is consistent with the conditions over Western India during DJF, when the convective stability is high, and subsidence is present as the prevailing flow moves from land to ocean [*Krishnamurti et al.*, 1997].

2.3. Interactions With the Arabian Sea Environment

[12] During prevailing winter monsoon flow regimes, it is likely that the aerosols from the Bombay Plume have the highest impact on the Arabian Sea. Aerosol particles in the atmosphere reduce the solar radiation reaching the surface. Many aerosol species such as black carbon and sulfates are strong absorbers of visible and near visible wavelengths compared to dust and sea salt. This has the effect of reducing the short-wave radiation that gets transmitted below the scattering particles [*Lau and Kim*, 2007; *Ramanathan et al.*, 2005]. This influence of aerosols

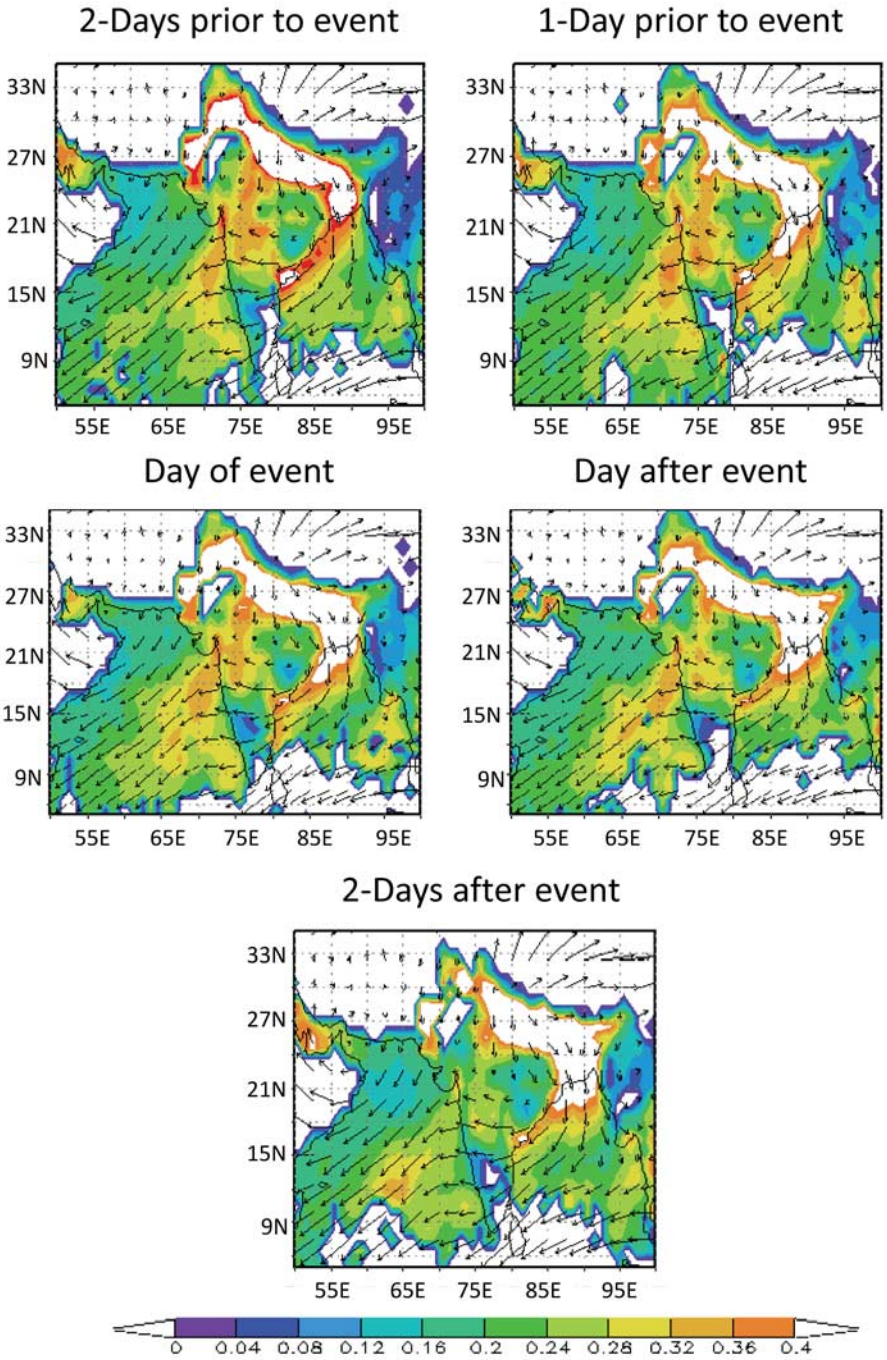

Figure 2. Composites of total AOD (at 550 nm) and 5-day mean of 925-hPa winds for each day of plume cases on 2003–2007 during DJF.

on the atmospheric radiation budget has been studied extensively. It has been linked to an ''Elevated Heat Pump'' over the Tibetan Plateau, and the weakening of tropical cyclones caused by lower sea surface temperatures [*Lau and Kim*, 2007; *Lau et al.*, 2006].

[13] A reduction of sea surface temperatures directly under high aerosol concentrations (high optical depth) was seen during the ''plume events'', even with the annual and seasonal cycles removed by a Fourier filter. However, this cooling cannot be entirely attributed to solar dimming. The region of the plume carries strong lower tropospheric winds that can also contribute to a cooling of the ocean from the surface wind stress curl and from surface fluxes of sensible and latent heat.

[14] It is accepted that atmospheric aerosols can have a large impact on cloud formation and precipitation microphysics, which in turn affects rainfall, cloud lifetime, and cloud-radiative forcing changes [*Takemura et al.*, 2007]. Certain aerosol species serve as CCN, and narrow the droplet size distribution within a cloud. For high aerosol concentration, more CCN are available for activation; hence more of them get activated to become cloud drops but with smaller drop sizes. This in turn hampers autoconversion as well as the subsequent collision/coalescence, which lead to

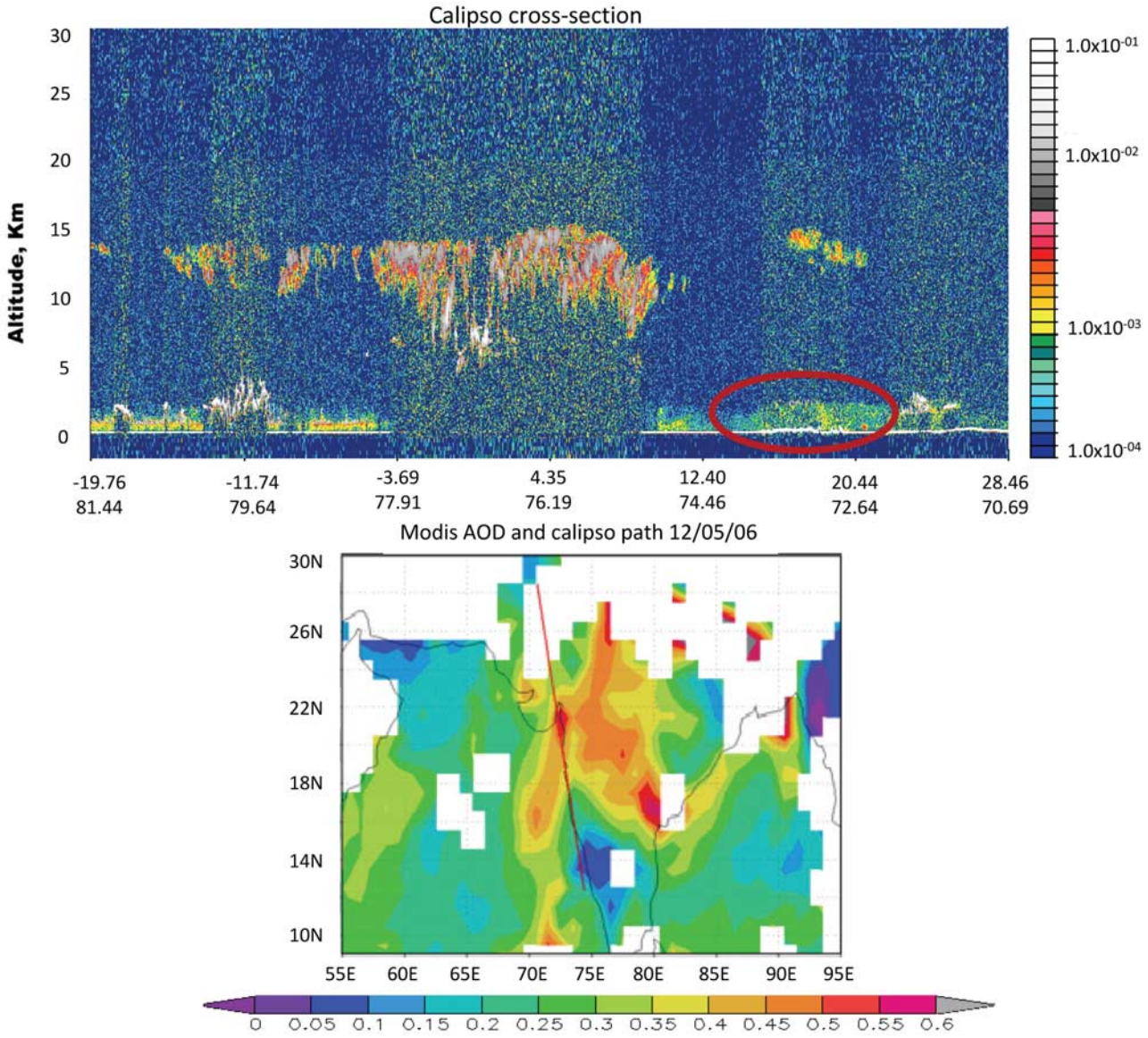

Figure 3a. Vertical backscatter from CALIPSO from 5 December 2006 (plume in red circle) and (bottom) plan view of CALIPSO's path (red line) over AOD on 9 January 2007. The negative numbers along the abscissa at the top denote southern latitudes.

the formation of raindrops [*Kaufman et al.*, 2005; *Sud and Lee*, 2007].

[15] Probability distributions for CER and COD were produced to examine the second indirect effect in the plume area. Since the BP existed only at low levels, only parameters of liquid phase clouds were extracted from the MODIS data. Sometimes an inconsistency between the cloud definition of MODIS and TRMM are noted. We have noted assignments of sky conditions designed as CER or COD when in fact TRMM (or ground-based observations) are calling for cloud conditions. This inconsistency may be related to sunglint [*Platnick et al.*, 2003]. To guard against it, TRMM cloud liquid water data was used as a cloud mask. A threshold value of TRMM liquid water content of 0.04 g/kg was used. Naturally, grid points with lower liquid water content were ignored.

[16] A treatment involving comparisons over successive 5-day periods, as done with SST and AOD was not valid for the cloud parameters due to the short timescale of cloud development and decay. Even using data combined from both MODIS satellites would exceed this timescale. To compare high aerosol (dirty) air and low aerosol (clean) air clouds, each Terra/Aqua pass was treated as a synoptic snapshot. Points with AOD > 0.5 were considered dirty, and points with AOD < 0.2 were considered clean. Grids were examined pass-by-pass and day-by-day for all DJF days from December 2002 to February 2007. After separation into clean and dirty categories, the grid points were passed through the cloud mask described above. Cloudy points were grouped into linearly spaced bins by CER or COD value.

[17] Figure 4 shows that the distribution of CER for dirty air is much narrower than for clean air. The mode of the distributions is identical, however, the distribution is

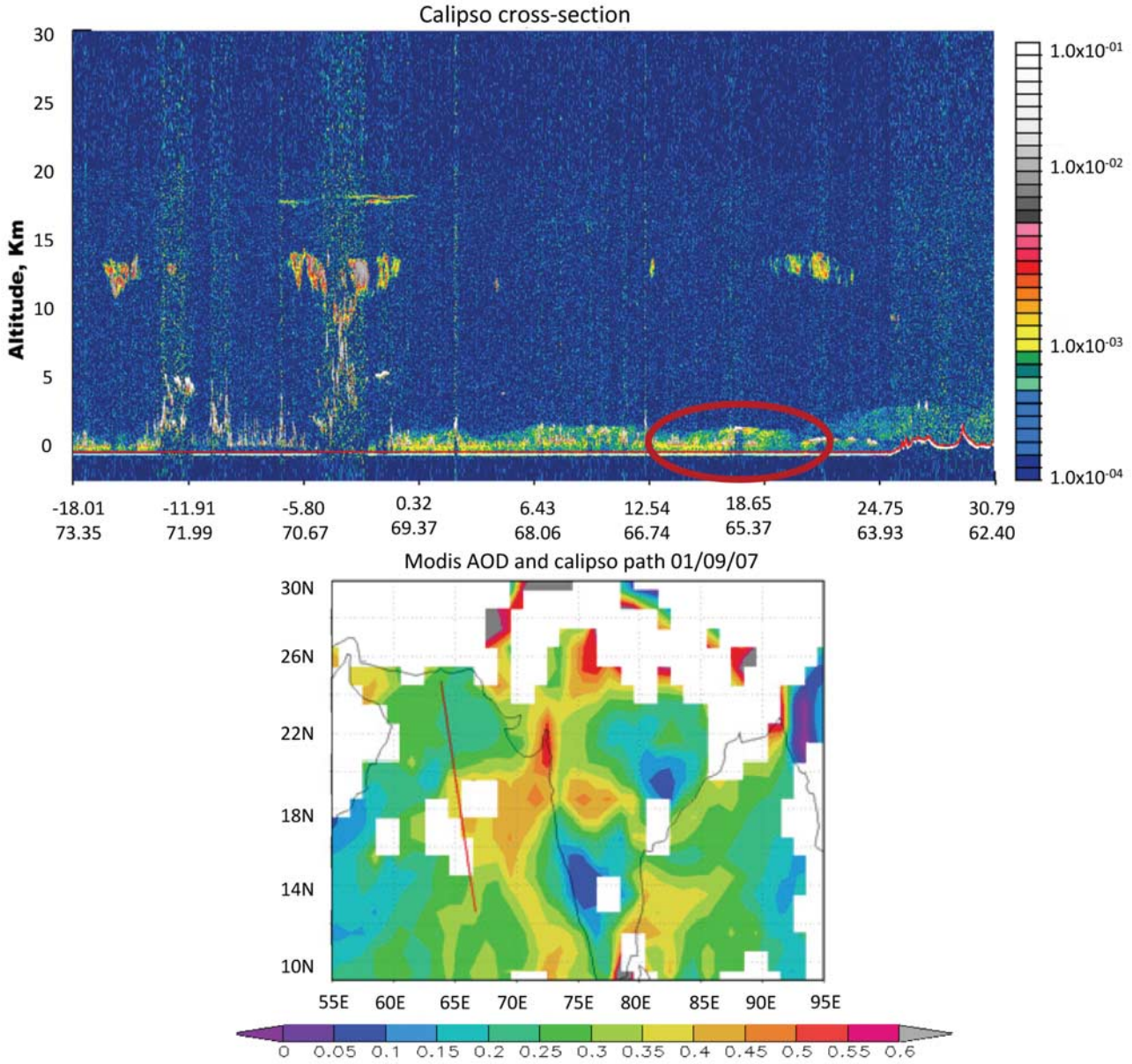

Figure 3b. Vertical backscatter from CALIPSO from 9 January 2007 (plume in red circle) and (bottom) plan view of CALIPSO's path (red line) over AOD on 9 January 2007. The negative numbers along the abscissa at the top denote southern latitudes.

skewed slightly toward smaller radii for the clean air. Figure 5 shows the distribution for cloud optical depth of clean versus dirty air. Both mode and bulk of the distribution is at higher COD for dirty air than for clean air, suggesting that the second aerosol indirect effect is causing more persistent low clouds where plume aerosols are present.

3. Model Used

[18] Our primary interest here is the direct and indirect effects of absorbing aerosols on the winter monsoon over the Arabian Sea, Bay of Bengal and southern India. We have used the NASA GEOS-4 AGCM to examine the direct and indirect effects of aerosols. This is a finite volume, grid point model with horizontal resolution of 2.5° in the east-west and 2.0° in the north-south directions (total 144 × 91 grid points). The model uses hybrid coordinates in the vertical with a total of 55 levels. The model uses the McRAS cumulus convection scheme [*Sud and Walker*, 1999a, 1999b] with further modification by *Sud and Walker* [2003a, 2003b]. The McRAS scheme is a modified version of the Relaxed Arakawa-Schubert (RAS) scheme by *Moorthi and Suarez* [1992]. The radiation parameterization is based on the works of *Chou and Suarez* [1994] and *Chou et al.* [1998].

3.1. Formulation of Aerosol Indirect Effects in the Model

[19] Aerosol-cloud interaction in the model is based on the work of *Sud and Lee* [2007]. This was designed to work

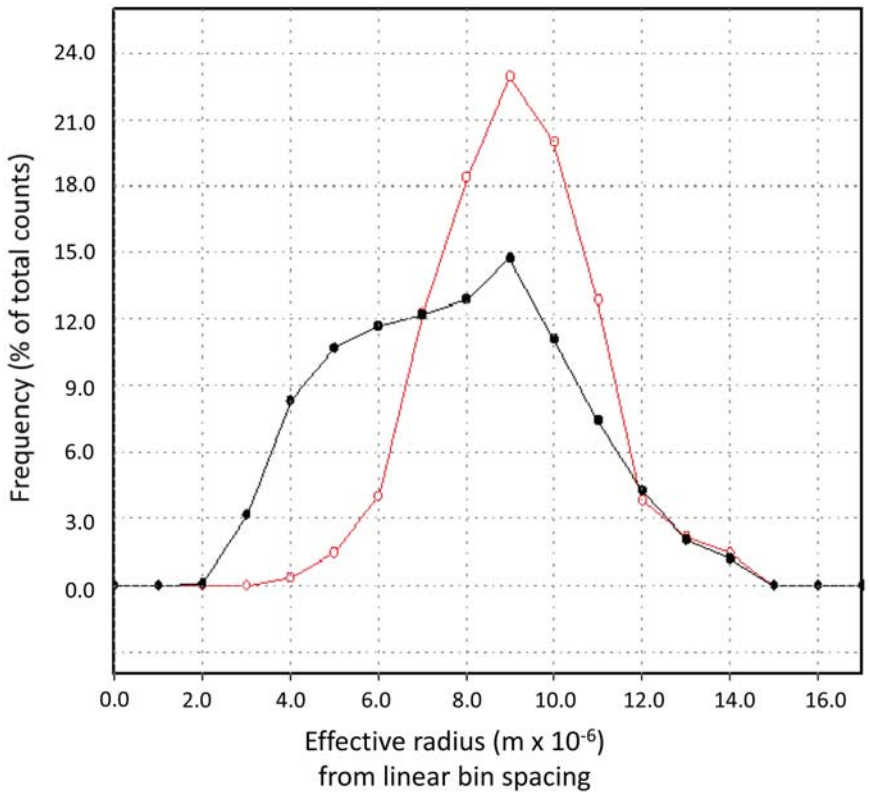

Figure 4. Probability distribution of MODIS-derived cloud effective radii for dirty air grid points (red) and clean air grid points (black). Taken from 8–18°N, 62–72°E during DJF 2003–2007.

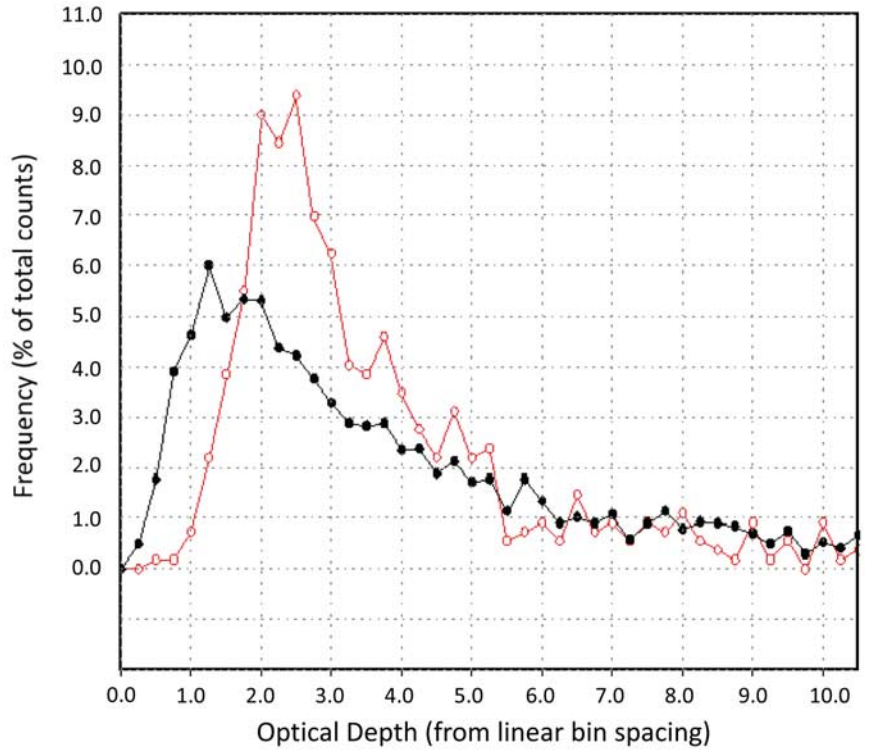

Figure 5. Probability distribution of MODIS-derived cloud optical depth for dirty air grid points (red) and clean air grid points (black). Taken from 8–18°N, 62–72°E during DJF 2003–2007.

Table 2. Details of Different Experiments

Dates	Number of Experiments: Indirect Plus Direct Effects	Number of Experiments: Indirect Effects Only
30 December 2002–8 January 2003	5 (with different initial conditions)	1
28 November 2003–7 December 2003	1	1
27 November 2005–6 December 2005	1	1
7 January 2006–16 January 2006	1	1
3 January 2007–12 January 2007	1	1
Total	9	5

with the McRAS [*Sud and Walker*, 1999a, 1999b]. The modified scheme along with aerosol activation (AC) algorithm will be referred as McRAS-AC. In McRAS-AC, the aerosol activation physics is based on the work of *Fountoukis and Nenes* [2005] and *Liu and Penner* [2005]; the aerosol-cloud microphysics is based on a modified version of the *Seifert and Beheng* [2001] scheme; cloud drop size distribution is based on the work of *Khvorostyanov and Curry* [1999a, 1999b]. The aerosol activation algorithm is capable of dealing with an entire spectrum of aerosols species. In our study, we have used five aerosol species, namely, black carbon, sulfate, dust, organic carbon and sea salt. The number of activated CCN is determined when the rate of change of supersaturation (S) of the cloud/air parcel is in steady state ($dS/dt = 0$) when the supersaturation S reaches the highest value as implemented by *Sud and Lee* [2007].

3.2. Formulation of Aerosol Direct Effect in the Model

[20] Aerosol direct effect is invoked through optical properties of aerosols [*Chou and Suarez*, 1994; *Chou et al.*, 1998]. The aerosol-radiative component in the model computes 11 short-wave band and 10 long-wave band aerosol optical properties for all of the five aerosol types (dust, black carbon, sulfate, sea salt, organic carbon). The aerosol-radiative effects vary diurnally with the solar zenith angle.

4. Simulation Experiments

[21] Five different 10-day periods in the 2002 to 2007 period in which Bombay Plume was significant were selected for the study. AOD averaged over the Arabian Sea was highest typically on the 6th day of a 10-day period. Simulations with the GEOS GCM started on day 1 and were continued through day 10 with the observed aerosol forcing in the model. Two sets of simulations were performed. The first one includes vertical distribution of aerosols from GOCART climatology and the second one includes observed aerosol from the MODIS data. Table 2 lists the details of these experiments. To assess the direct and indirect effects of aerosols separately, two sets of simulations using both climatological and MODIS aerosols were performed. One invoked both the direct and indirect effect of aerosols and the other had only the indirect effect of aerosols. We found that the direct and indirect effects of aerosols are most pronounced from days 6 to 10 of forecasts. We noted small differences between the control and the MODIS runs during the first 5 days of integration. The effects of heavy pollution show a slow spin up and we noted that the difference between the control and the MODIS runs were more discernible after 5 days of integration. Initial conditions were taken from NCEP/NCAR reanalysis project. SST surface boundary conditions were taken from the work of *Reynolds and Smith* [1994] weekly data sets and were interpolated linearly to the model simulation time. In addition, four more simulations were performed with perturbed (surface) initial conditions during 2002/2003 winter season with both direct and indirect effects of aerosols included.

5. AODs From MODIS for Modeling Case Studies

[22] We have selected several cases, each covering a duration of 10 days, that exhibited large AODs, as seen from MODIS data sets, over the Arabian Sea. These are illustrated in Figures 6a–6e. Figure 6a shows a case from 30 December 2002 through 8 January 2003. Here an increase of AOD to almost 0.45 units over the Central Arabian Sea is seen. This case can be characterized as a Bombay Plume that emanated from the northwest coast of India and extended south to southwestward into the central Arabian Sea. This period was selected for exploring model sensitivity to AOD increases. A corresponding period in the year 2003 (Figure 6b) was from November 28 through December 7. The plume extended southwestward from the west coast of India and made its way over the central Arabian Sea in the 10-day period. The largest magnitude of the AOD was ~0.40. Large accumulation of AOD over northwestern India preceded most of the Bombay plume events. Figure 6c illustrates the third case (27 November–6 December 2005). In all these cases the accumulation of large AOD over the Central Arabian Sea near 10N was noted. A moderate increase of AOD between 7 January 2006 and 16 January 2006 featured in Figure 6d, where the AOD showed increases over the near-equatorial latitude belts over the western Arabian Sea. A decrease in AOD was noted from 14 to 16 January 2006. A spectacular case of southward emanating Bombay plume was noted between 3 and 12 January 2007 (Figure 6e). Thereafter this plume extended southwestward as it weakened. Most of the central Arabian Sea was affected by increased pollution during this event when the largest values of AOD reached values as high as 0.40 units. The above five cases are typical of heavy pollution episodes that start with an accumulation near the west coast of India and proceed southwestward extending over the Arabian Sea.

[23] In the absence of key aerosol species in the MODIS data, we took the well-validated GOCART aerosol climatology [*Chin et al.*, 2002] and scaled the vertical distribution of five aerosols: black carbon, sulfate, dust, organic carbon and sea salt. We plotted them over the Arabian Sea (50–75E, 0–20N). The results for all cases were quite similar in that the AOD for all aerosol species for the MODIS data showed larger aerosol content at all the vertical levels as compared to GOCART. The differences are shown in Figure 7.

[24] Over the Arabian Sea (50–75E, 0–20N) the MODIS based AOD was noted to increase. These are shown in Figures 8a–8e covering the 10-day periods for the five cases from 2002 to 2008. For most cases AOD over the

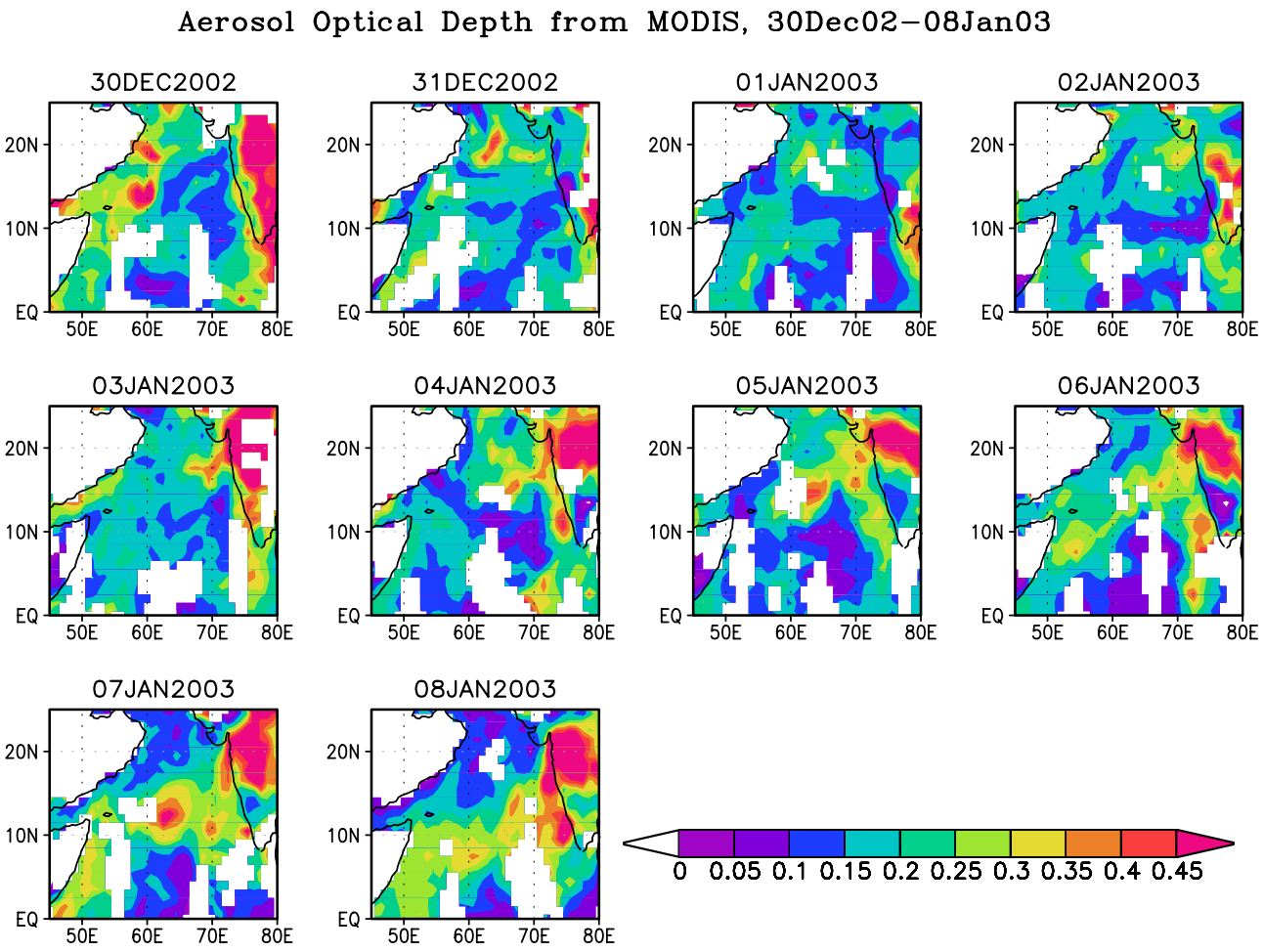

Figure 6a. AOD from MODIS during 30 December 2002 to 8 January 2003 over Arabian Sea.

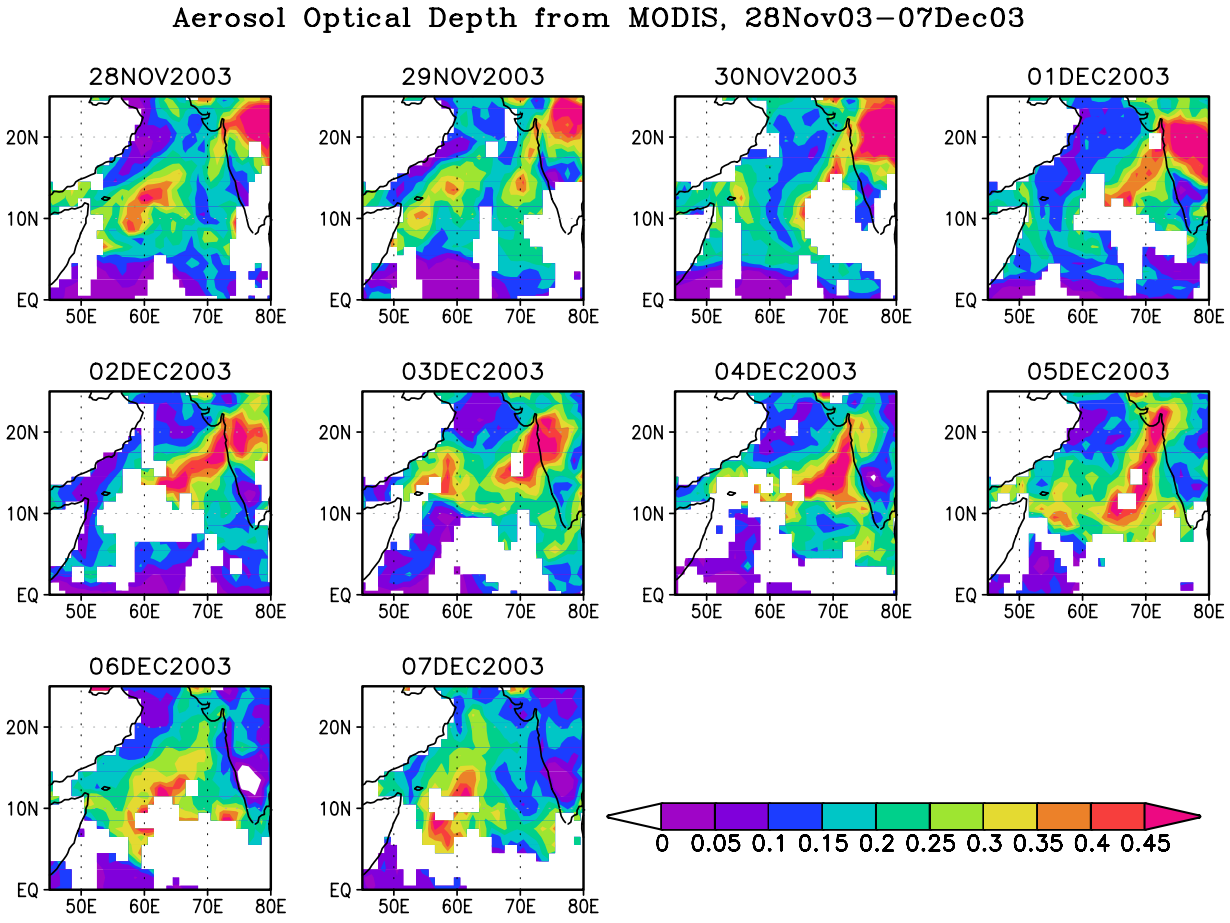

Figure 6b. AOD from MODIS during 28 November 2003 to 7 December 2003 over Arabian Sea.

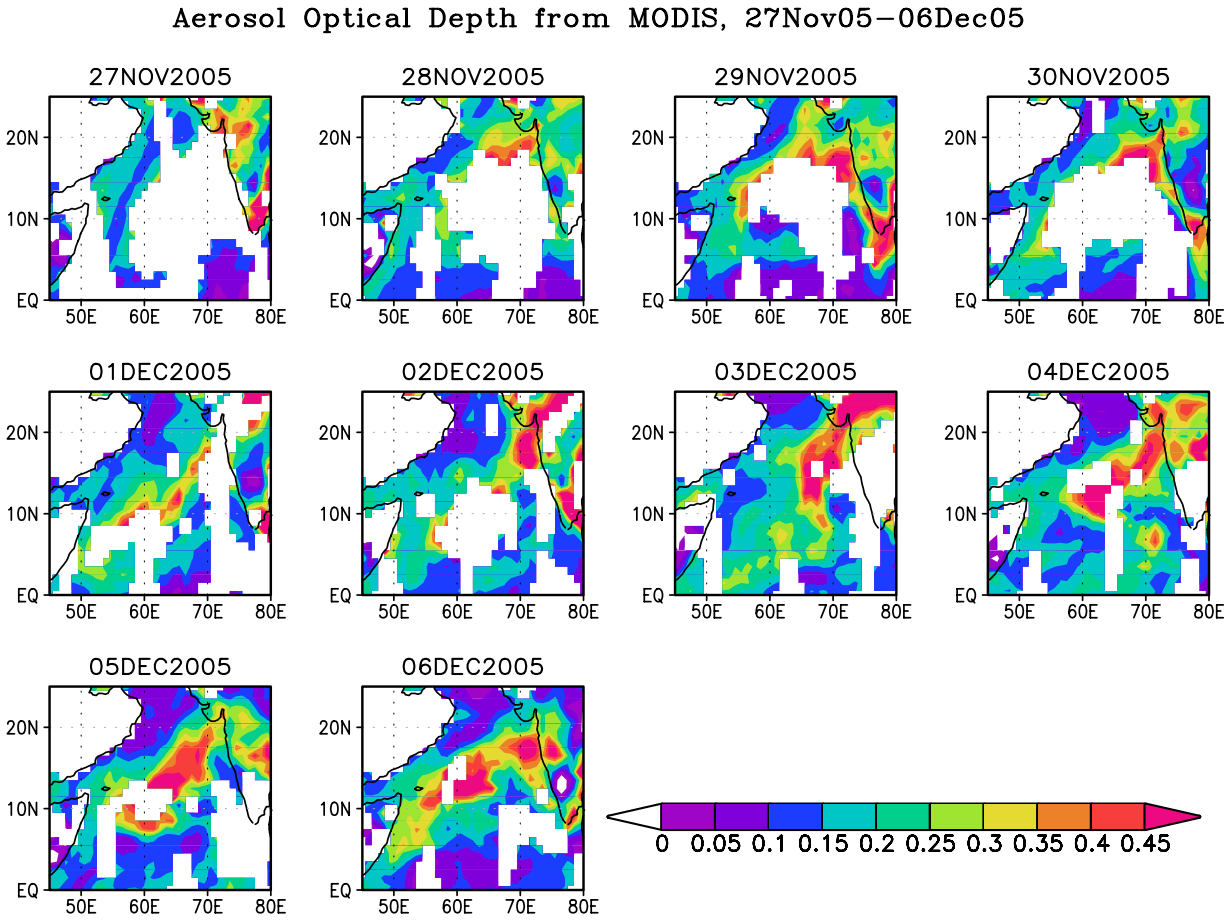

Figure 6c. AOD from MODIS during 27 November 2005 to 6 December 2005 over Arabian Sea.

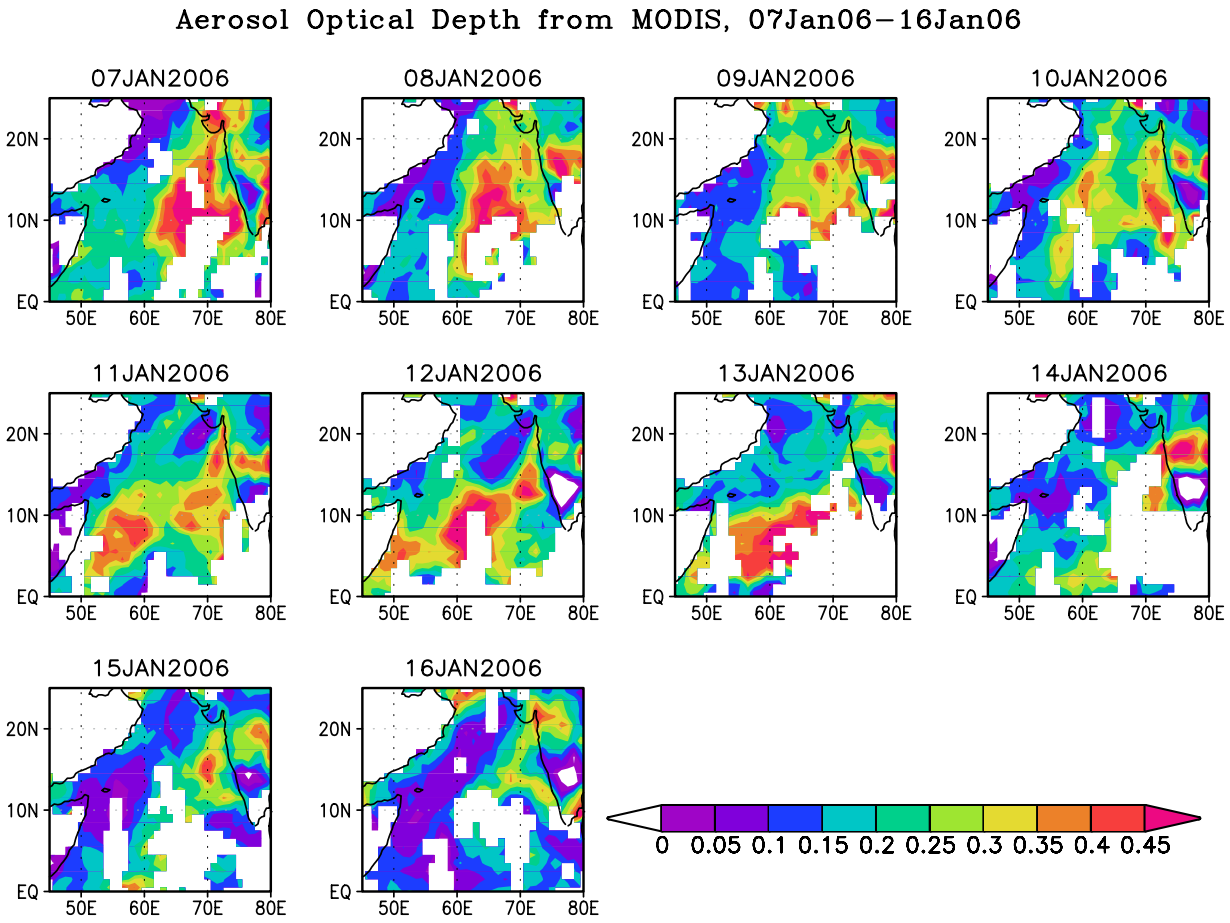

Figure 6d. AOD from MODIS during 7 January 2006 to 16 January 2006 over Arabian Sea.

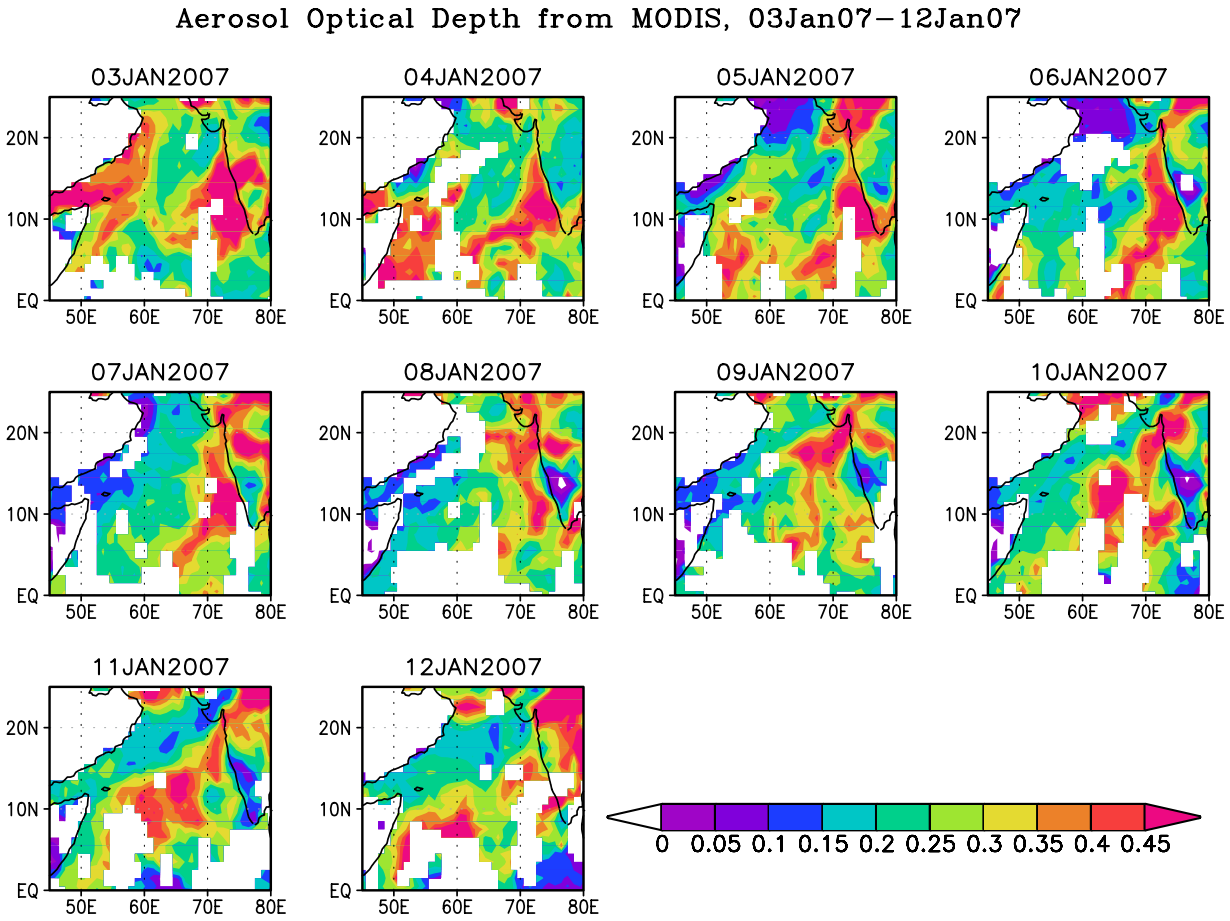

Figure 6e. AOD from MODIS during 3 January 2007 to 12 January 2007 over Arabian Sea.

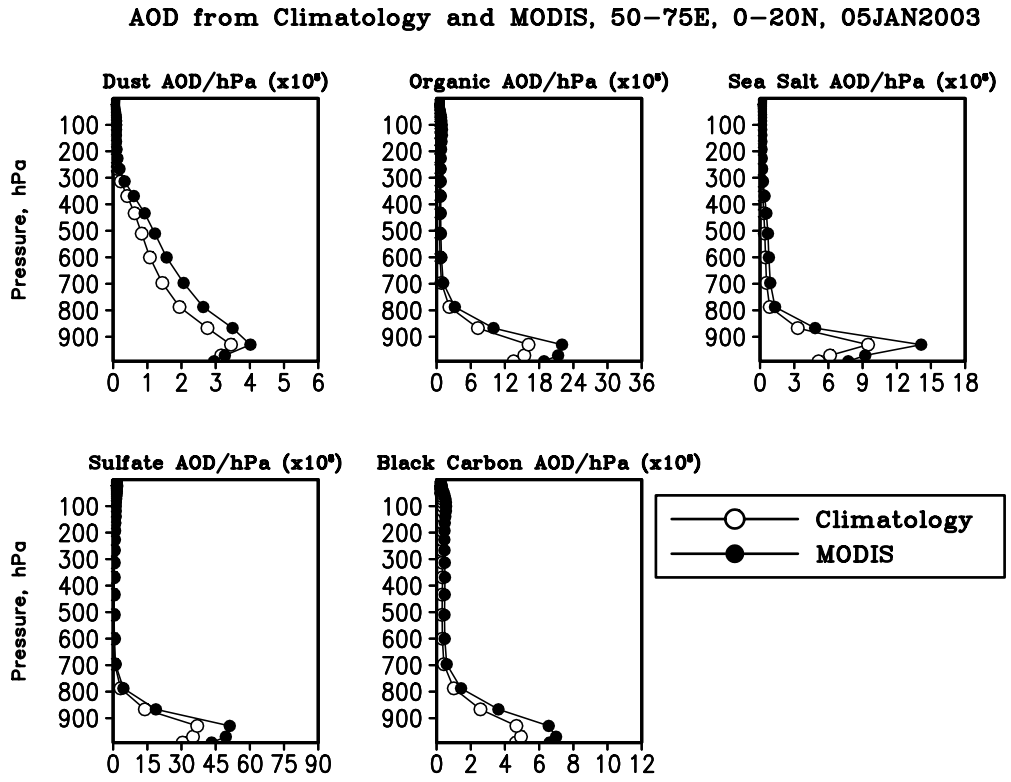

Figure 7. Vertical distribution of AOD of five different aerosol types averaged over the Arabian Sea (50–75°E, 0–20°N) on 5 January 2003 as obtained from climatological data derived by the GOCART model and MODIS satellite observation. Vertical distribution of different aerosol types from MODIS was obtained by using the weights of GOCART climatology.

Arabian Sea was strongly influenced by the Bombay plume. There were two cases in which the AOD was somewhat different in character during the respective 10 days because of the trajectories of the Bombay plume. Overall, AODs ranged around 0.22 to 0.24 units when the aerosols impacted the central Arabian Sea. The climatological values of AOD from the NASA's reference model GOCART from November through February for the Arabian Sea (50–75E and 0–20N) are shown in Figure 8f. Evidently, these values are much lower than those of the MODIS cases shown in (Figures 8a–8d and 9e). Climatological values of AOD increase by about 20% between January and February. The MODIS events carry heavier aerosols compared to the climatological values and their influences on the simulations are a key focus of the study.

6. Results

[25] In Figure 9 we show the averaged rainfall over the entire Arabian Sea for all the nine simulations (five different initial conditions during 2002 and one each during 2003, 2005, 2006 and 2007) for the first 5 days (days 1–5 of forecasts; left) and the second 5 days (days 6–10; right) using both the aerosol direct and indirect effects. Figure 9 shows a comparison between the control GOCART runs with the MODIS case studies. We note a very small difference in the first 5-day rainfall totals. Nevertheless, there is an increase in rainfall totals for the second 5-day period (days 6–10 of forecasts.) Averaged over the entire Arabian Sea, the 5-day impact on precipitation totals is on the order of 0.25 mm/day, however, as seen previously, enhancement of precipitation from aerosols over the selected regions was as high as 3 mm/day.

[26] The rainfall totals from the indirect effects (excluding the direct effects) are shown for similar area averages for the entire Arabian Sea in Figure 10. These results confirm that the sensitivity from the aerosol effects for the MODIS cases are also seen when the indirect effects alone are considered. It should be noted that the Arabian Sea is not a region of heavy rains during the winter monsoon season. This is a region where a large concentration of pollutants is seen. We see the impact of the aerosol effect on the smaller rainfall totals over this region.

[27] In the rest of this study we show the sensitivity of rainfall to aerosol mass concentration over the entire Arabian Sea. Figure 11 shows precipitation differences between the GOCART and MODIS aerosol forcing (both direct and indirect effects). Arabian Sea rainfall increases in excess of 3 mm/day in most of these MODIS experiments for forecasts between day 6 to day 10. A departure by ±0.5 mm/day depicted by light blue and yellow colors is close to the normal climatological reference. Thus when the direct and indirect effects are both included in the MODIS simulations, the influence of Bombay Plume is to produce a large increase in rainfall. It is more discernible over the ocean because the climatological aerosols over the ocean are small and an enhancement in their concentration by Bombay Plume produces a large impact. The different panels of Figure 12

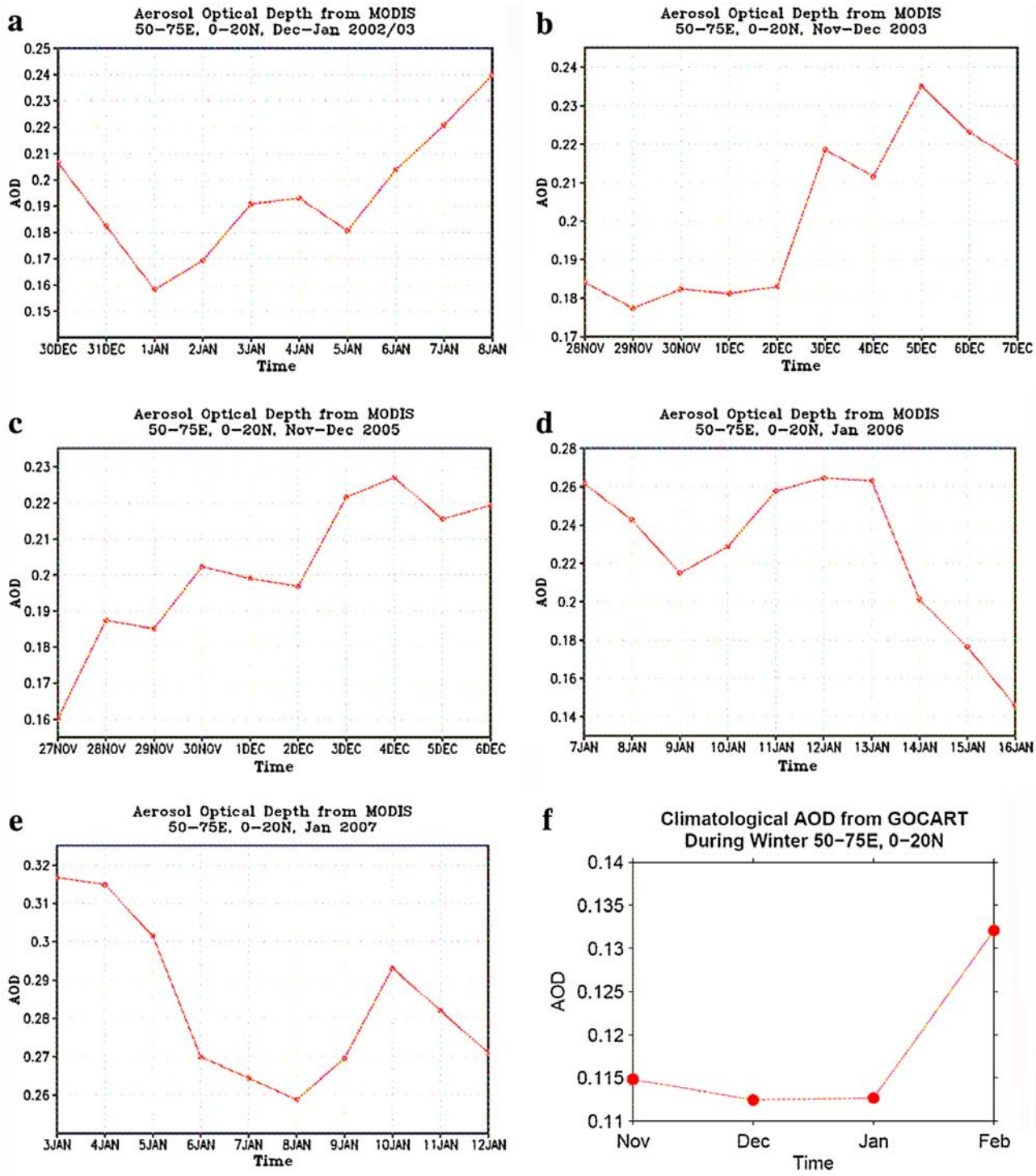

Figure 8. Time series of total AOD from MODIS during the five 10-day periods of our study averaged over the Arabian Sea (50–75°E, 0–20°N). And time series of total AOD from GOCART (climatology) during November–February over the same region.

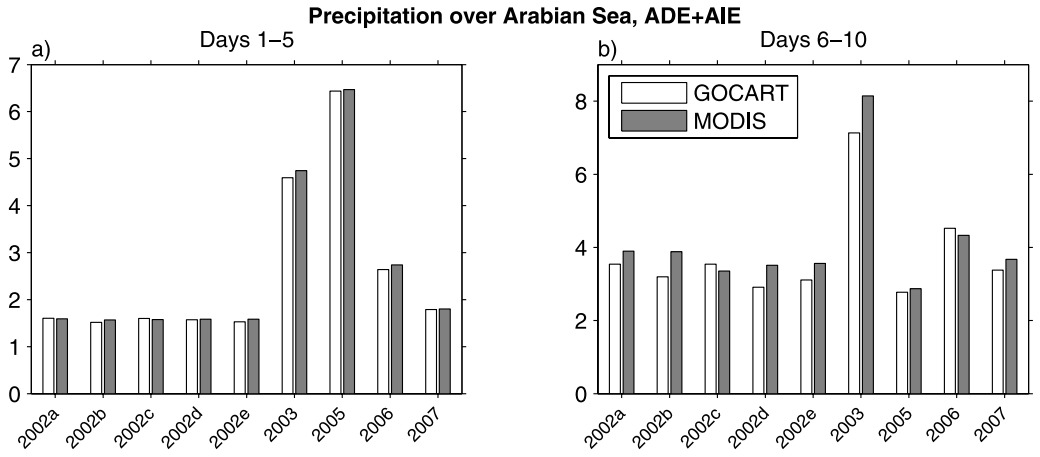

Figure 9. Precipitation (mm/day) over the Arabian Sea (50–75°E, 0–20°N) using GOCART (climatological) and MODIS aerosols in the GEOS model that includes both direct and indirect effects: (left) days 1–5 and (right) days 6–10.

show results that are similar to those presented in Figure 11. In all these cases we see an enhancement of rains over the Arabian Sea when the heavy aerosol effects are included.

[28] A new result of our study is the aerosol induced east-west circulation, which works as follows. When the aerosol induced rains (MODIS minus Control) became larger in the Arabian Sea for days to 6 through 10 of forecasts (averaged over all Simulations), there was a reduction of rains over the Bay of Bengal. Both the positive and negative changes were of the order of 3.0 mm/day (Figure 13). In this diagram we show the ensemble mean rains for MODIS minus the Control for the simulations that included the direct plus the indirect effects (all nine members, top). This east-west difference between the Arabian Sea and the Bay of Bengal was also seen in all individual cases in the 5 years (bottom). It appears that the increased rain and the increased aerosol heating induce a local east-west circulation with the ascending lobe in the regions of enhanced heating over the Arabian Sea. In Figure 14 we show the aerosol heating-induced divergent circulation anomaly and its winter monsoon rainfall impacts. As a consequence of the aerosol heating over the Arabian Sea (where the aerosols were noted to accumulate), a rising motion anomaly is found over this region. This is most evident in the comparison of the results of the MODIS based experiments (that included the direct and indirect effects) to the control run (GOCART) that included climatological aerosols. The velocity potential anomaly (MODIS minus GOCART) at the 200-hPa level (Figure 14a) shows that the convergence center over the Bay of Bengal is accompanied by a compensating descending lobe (induced by the ascending lobe of the Arabian Sea). The size of the ascending and the descending lobes are similar. The intensity of the induced downward motion is on the order of 1 cm/s. The anomaly can potentially suppress the winter monsoon rains. The following interpretation of the velocity potential isopleths and maximum divergence ($-\nabla^2\chi > 0$) is important. When one sees a near circular pattern of a stream function ψ, the stream function mini-

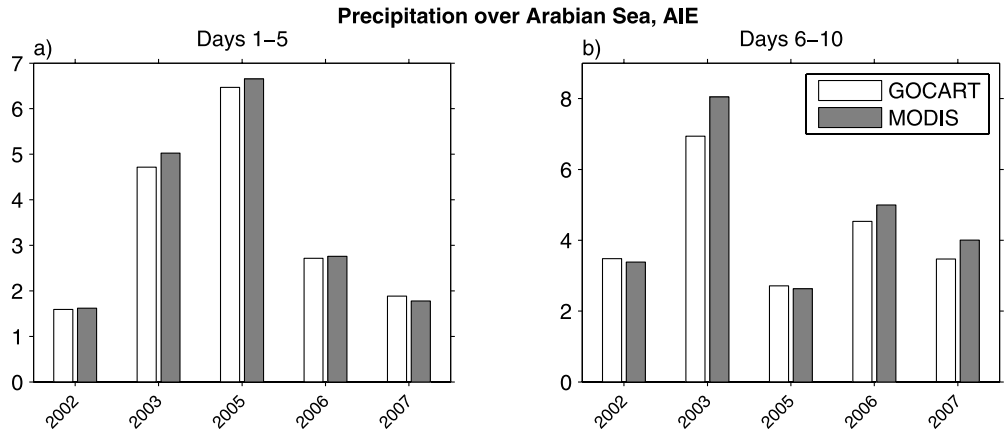

Figure 10. Precipitation (mm/day) over the Arabian Sea (50–75°E, 0–20°N) using GOCART (climatological) and MODIS aerosols in the GEOS model that includes only indirect effects: (left) days 1–5 and (right) days 6–10.

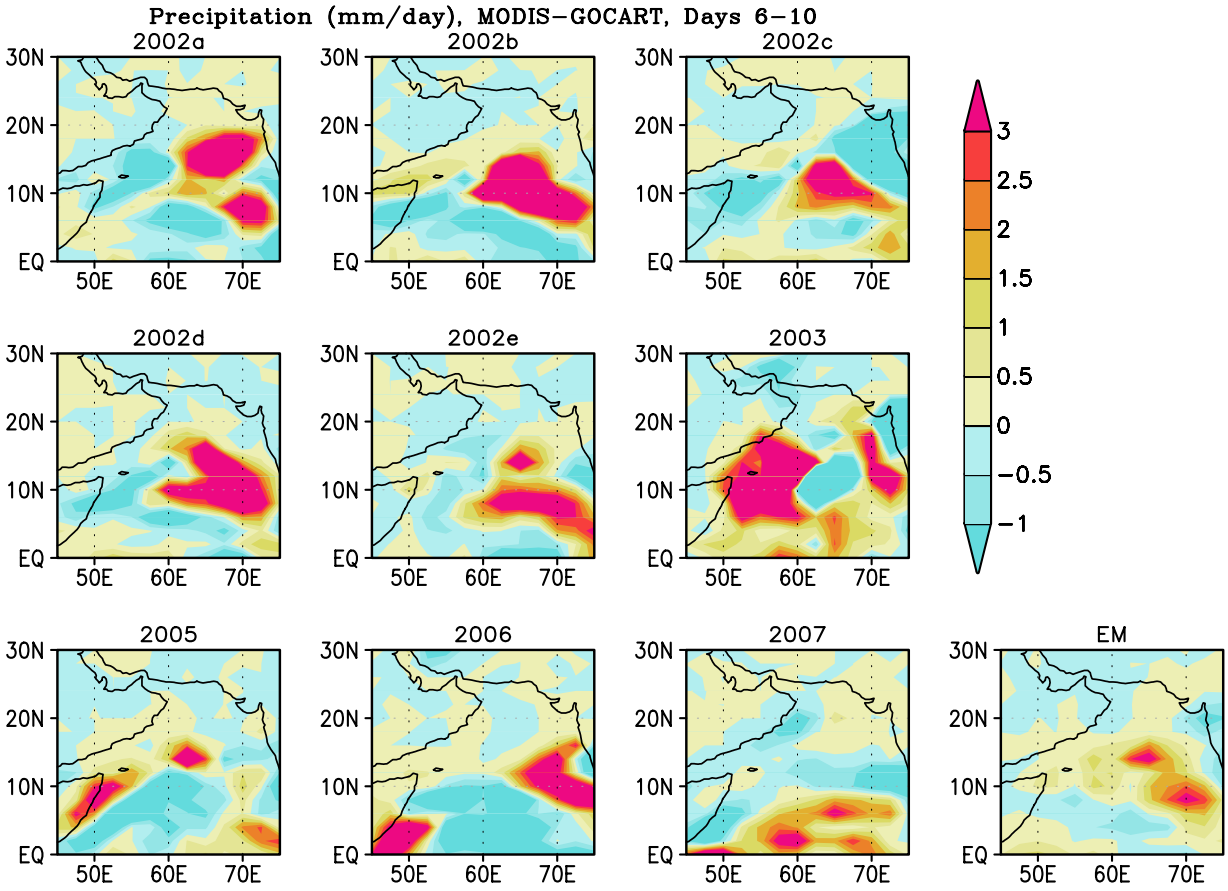

Figure 11. Difference in precipitation during days 6–10 from all the nine members with both direct and indirect effects of aerosols obtained from GOCART climatology and MODIS observations during 2002–2007. EM, ensemble mean of all the nine members.

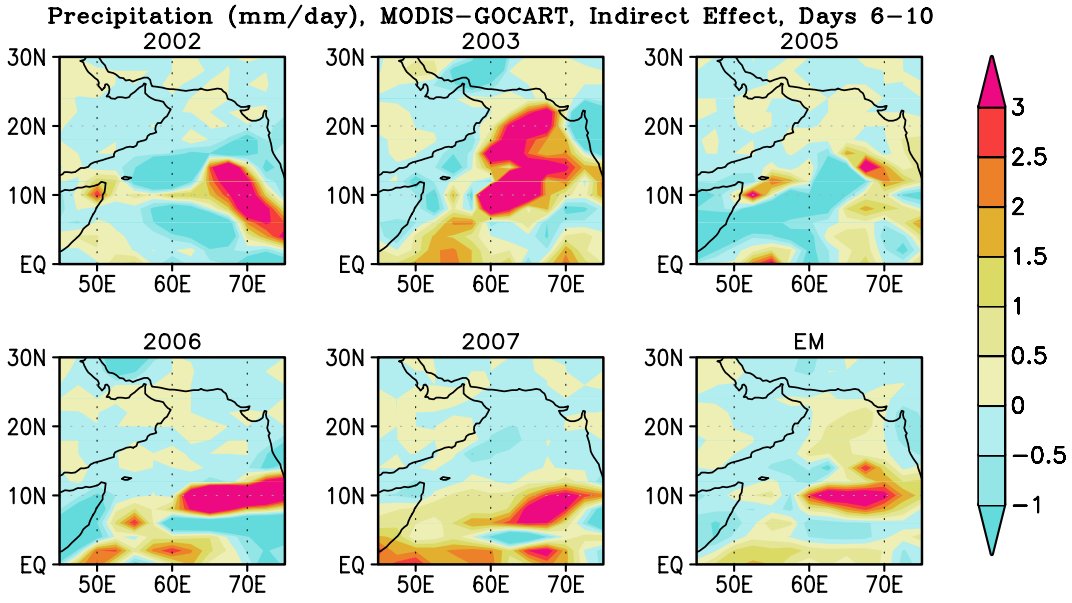

Figure 12. Difference in precipitation during days 6–10 in five different years of simulations with only the indirect effects of aerosols obtained from GOCART climatology and MODIS observations. EM, ensemble mean of all the nine members.

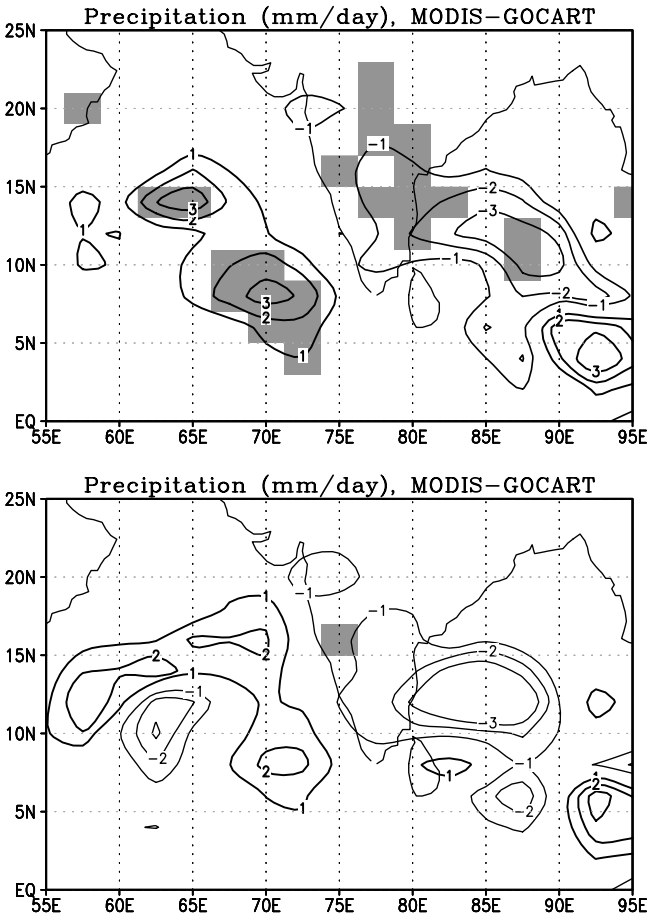

Figure 13. Difference in precipitation over the Arabian Sea and Bay of Bengal from the ensemble mean of (top) nine members with both direct and indirect effects of aerosols and (bottom) five members. The regions wherein the difference was significant with more than 95% confidence are shaded.

mum (at the center of the circular pattern of ψ) does not necessarily coincide with the region of largest vorticity $\nabla^2\psi$. The Region of largest vorticity lies in regions where the shear plus curvature vorticity of the rotational flow provides a maximum. The region is generally located over the region of strongly curved and placed ψ isopleths. The same type of interpretation is needed for relating χ maximum and the region of maximum divergence ($-\nabla^2\chi > 0$) and vertical motion. Although the χ maximum is located over Saudi Arabia (Figure 14a), the maximum rising motion are shifted to the northeast where the placing of the χ isopleths are the largest. A similar interpretation should be used for the Bay of Bengal region. It should be noted that these are anomalous ascending and descending lobes induced by the aerosol heating over the Arabian Sea and disappear if MODIS pollutions is removed. Figure 14b shows the east-west circulations that suppress the Bay of Bengal rains somewhat, thus manifesting a negative rainfall anomaly. Figure 14c shows the reduction in the coastal winter monsoon rains over southeast India. We note that the reduction of rains for days 6 to 10 of forecasts were of the order of 4 mm/day along the Bay of Bengal coast where the climatological rains are the largest during the winter monsoon. This suggests that accumulation of pollution over the Arabian Sea can affect the intensity of winter monsoon rains on the Bay of Bengal coast.

[29] In recent decades Arabian Sea pollution has been increasing. One naturally wonders if there has been any measurable reduction of observed rains along the Bay of Bengal coast of India. Thus we examined the raingauge-based data archive using 23 recent years of daily precipitation. We examined possible linear trends of December–January rains (Figure 14d). A small measurable decreasing trend of rains is seen. We cannot attribute this trend entirely to the increasing pollution over the Arabian Sea due to large interannual variability of the rains in the region. Nevertheless, the influence of increasing Arabian Sea pollution, as a contributor to this trend, is supported by our simulation results. Further research will be needed to reaffirm these findings.

[30] The typical daily variability of the AOD (as seen from MODIS) for the winter seasons of the years 2000/2001 to 2003/2004 is shown in Figure 15a. This covers the Arabian Sea domain during the months of December (preceding year) and January (following year). AOD typically varies from 0.1 to 0.4 in this illustration. In order to find out if there is an indication of the response of rains over the Bay of Bengal during peak AOD events over the Arabian Sea (Figure 15a), we have plotted a composite of the precipitation along the Bay of Bengal coast for 1 day after the peak AOD days (Figure 15b). We decided to examine the Bay of Bengal rains for 1 day after the day of maximum pollution over the Arabian Sea to take into account the response time of aerosol forcing. We also show the climatological mean rainfall for the same calendar days of heavy pollution dates (plus one day) covering 30 years of observed rainfall. We note measurable reductions of the Bay of Bengal coastal winter monsoon rains during periods of high pollution. Those domain-averaged rain show nearly a 60% reduction in rains compared to climatology. We view this as observational evidence of reduction of winter monsoon Bay of Bengal rains following high pollution days over the Arabian Sea.

[31] A slight increase of cloud cover (roughly 1%) was noted over the Arabian Sea. This was the difference in cloud covers between the MODIS and the control experiment. This is largely reflected for the middle clouds (between the 600 and 400 hPa levels). In Figure 16 we show the results for all the nine members, the five models run for the year 2002 and for the five members during the five different years of simulations. All of these results are consistent and show that a small increase of cloud cover is related to the aerosol heating and associated rising motions. This heating in the lower troposphere due to MODIS aerosol forcing is shown in Figure 17 during days 1 through 5 of simulations. We have not shown the change in air temperature during days 6 through 10 because in this period the modified precipitation and circulation determines the heating rate. We have also noticed a small decrease in the cloud amount over the Bay of Bengal due to MODIS aerosol forcing when compared to the climatology (not shown). The increase of cloud amount over the Arabian Sea is consistent with the increase of convective cloud liquid water activation from the aerosol effect. The increases were on the order of

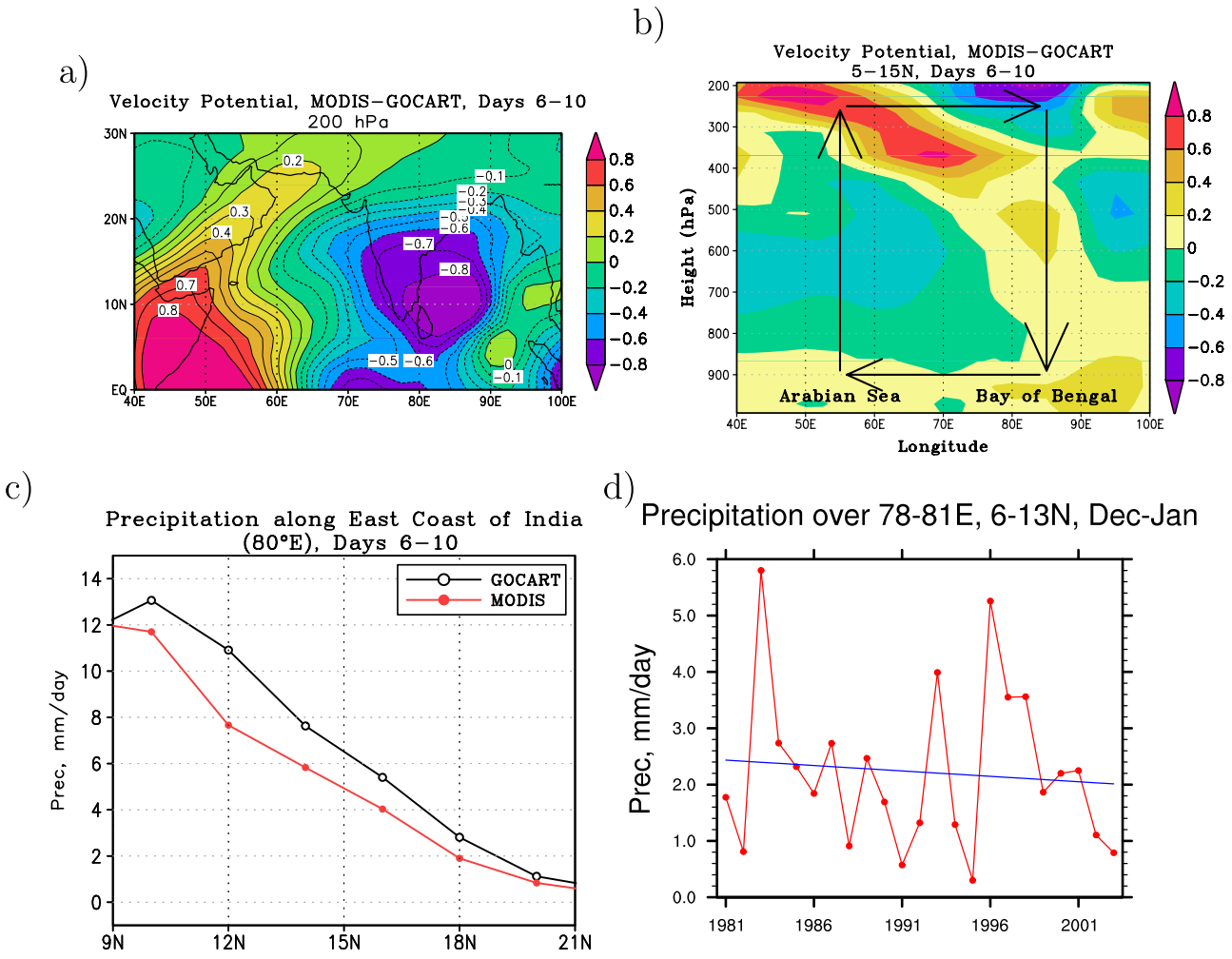

Figure 14. (a) Difference in velocity potential ($\times 10^{-6}$ s^{-1}) between GOCART and MODIS aerosol forcing at 200 hPa during days 6–10 of forecasts. (b) Difference in velocity potential ($\times 10^{-6}$ s^{-1}) between MODIS and GOCART aerosol-induced experiments averaged over 5–15°N during days 6–10 of forecasts. A relative positive velocity potential signifies relative divergence. Figure 14 shows that increased convection over the Arabian Sea forms an anomalous east-west circulation with descending motion over the Bay of Bengal. (c) Precipitation along 80°E from GOCART and MODIS aerosol forcing during days 6–10 of forecasts. (d) Mean precipitation during December–January 1981/2008 through 2003/2004 over the southeast coast of India (78–81°E, 6–13°N) from IMD observations. The linear trend in the precipitation over this region is shown in blue line (slope = ~0.02 mm day^{-1} a^{-1}).

200 CCN per cubic centimeter (Figure 18). The large increase between 900 and 500 hPa levels was noted in the model runs. The largest increase was found at the 500 hPa level where it impacted the middle cloud coverage.

7. Conclusions

[32] The Bombay Plume carries high aerosol concentrations during the winter monsoon months. The plume originates in West Central India near the cities of Mumbai/Pune and contains a high concentration of <0.5 μm size aerosol particles of largely anthropogenic origin. During typical DJF months, aerosols in the plume are transported over the Arabian Sea, but do not reach a height of more than 3 km as noted from CALIPSO profiling of aerosols. Although the observed bombay plumes over the Arabian Sea extend only to the 3-km level roughly, the coarse resolution global model used in the modeling study utilizes a PBL and a cumulus parameterization scheme that identifies a tropical cloud base near the 1-km level. The absorbing aerosols contribute to a heating and slow enhancement of buoyancy of the rising air, this is effective in enhancing the convective rains from the McRAS cumulus convection scheme. When the Bombay Plume is over the sea, high AODs persist for about 5 days. A typical BP is associated with a low-level northeasterly jet, which stretches across the entire Arabian Sea.

[33] While the cloud effective radius did not change much (increase or decrease) as a consequence of BP, a narrower distribution of effective radii was observed in areas affected by high aerosol concentration. As the average effective radius over a 1 × 1° grid is indicative of the type of cloud

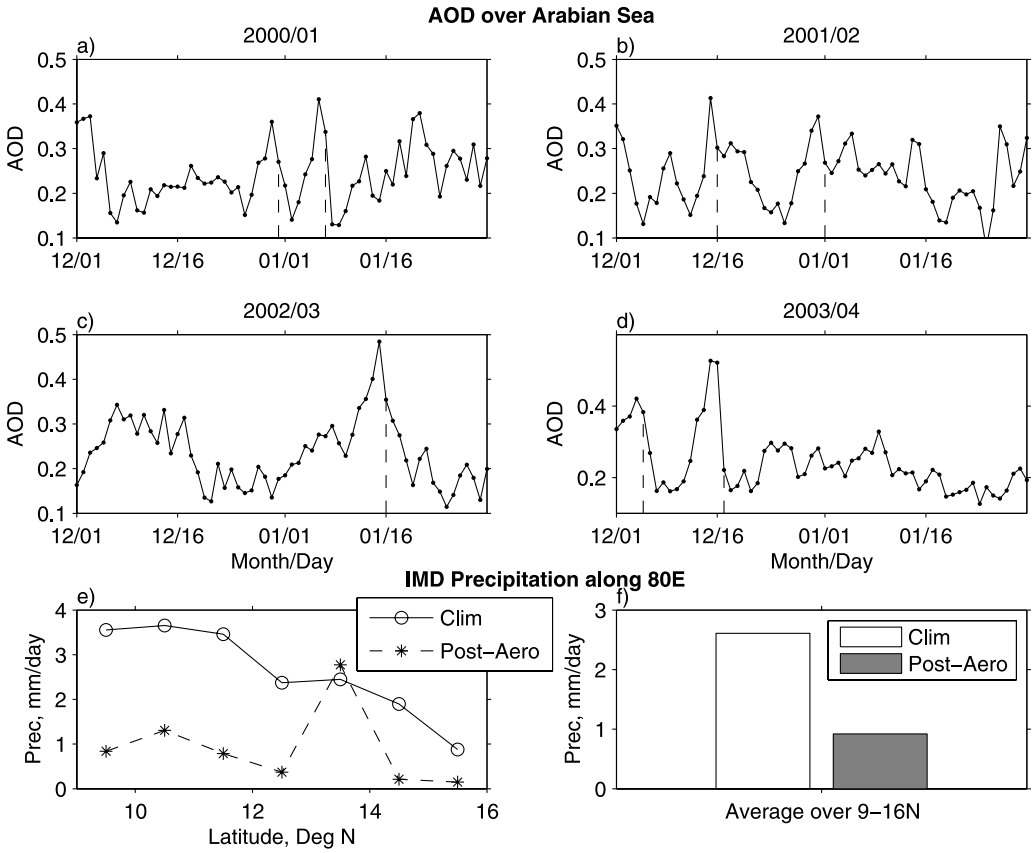

Figure 15. (a–d) AOD from MODIS over Arabian Sea during 2000/2001 to 2003/2004 winter seasons. The days considered for precipitation composites are indicated by dashed vertical lines (1 day after aerosol peak). (e–f) Precipitation climatology and postaerosol (1 day after the peak) composites of precipitation along 80°E.

present in the grid square, a narrower CER distribution suggests that there are fewer types of clouds present over that grid square. The distribution of cloud optical depth suggests a shift to more persistent clouds in high AOD areas. This is most likely at the expense of deep convective clouds, which have shorter lifetimes. More persistent low-level clouds over the EAS during winter will have a large impact on the radiation budget in the area. This shift in the radiation budget can be expected to have a significant impact on regional circulation and rainfall patterns in South Asia.

[34] Inclusion of these aerosols in the NASA/GSFC GEOS-4 general circulation model shows an increase in winter monsoon precipitation over the Arabian Sea during

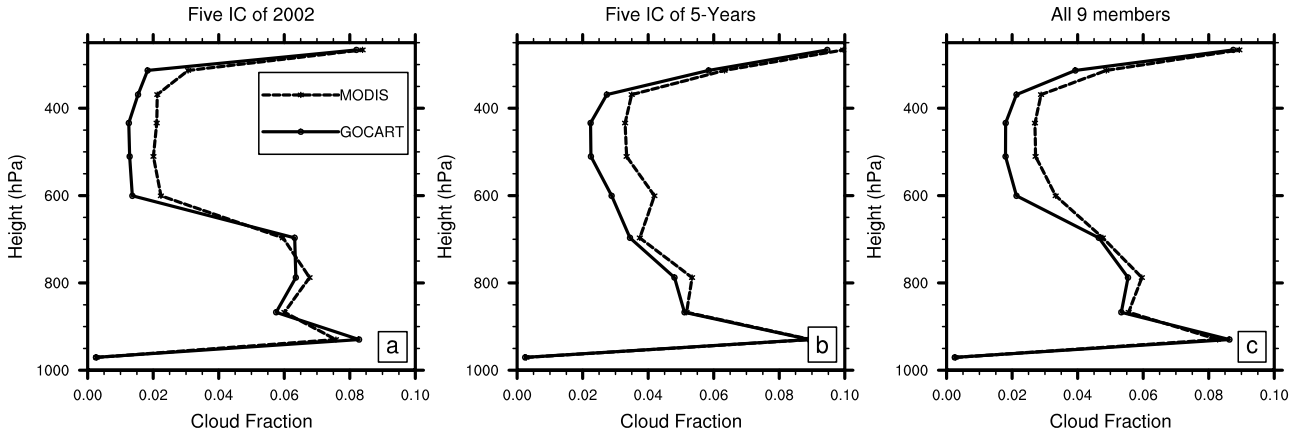

Figure 16. Cloud fraction over Arabian Sea from GOCART (climatology) and MODIS aerosol forcing for (a) all the five experiments during 2002, (b) for all the five experiments during 5 years, and (c) for all the nine member simulations during the 5 years.

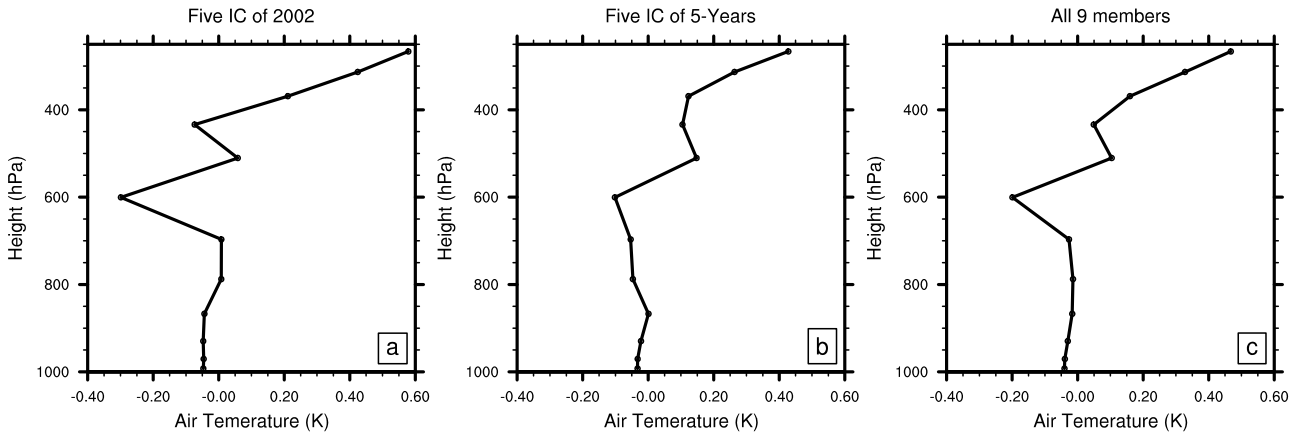

Figure 17. Change in air temperature over the Arabian Sea due to the effect of MODIS aerosol as compared to the GOCART climatological aerosol forcing during days 1–5 of simulations for (a) all the five experiments during 2002, (b) for all the five experiments during 5 years, and (c) for all the nine member simulations during the 5 years.

all the five years (2002, 2003, 2005, 2006 and 2007) when compared to that of the climatological aerosol effects. This increase in precipitation was evidenced when direct plus indirect, as well as only indirect effects were included in the model. The change in the amount of precipitation was much less during days 1–5 of simulations. However, the difference increased significantly in the second half of the 10-day long simulation. The increase in precipitation over the Arabian Sea induces an anomalous convergence near the surface and divergence in the upper troposphere. Descending motion over the Bay of Bengal compensates this anomalous ascending motion with a closed east-west anomalous circulation loop. These features disappear if the MODIS based pollution is not invoked in the simulation.

[35] During DJF simulations, thick aerosol clouds originating from west-central Indian industrial regions traverses over the Arabian Sea with the prevailing low-level wind field. Even though the parameterizations of the influence of aerosols on clouds and precipitation is not well developed, the aerosol cloud parameterizations of the aerosol direct and indirect effects are reasonable in the sense that they capture the influence of aerosols (from radiation and cloud effects) in numerical models [*Sud and Lee*, 2007]. This is evidenced from the enhancement of rain from the aerosol effects of excessive pollution over the Arabian Sea. The results presented here on the model-simulated impacts on the Bay of Bengal rain for the excessive Arabian Sea pollution rely a lot on the parameterization of aerosol effects in the GEOS-4 GCM using the McRAS-AC scheme. The observational evidence based entirely on the MODIS data inferred pollutants and the raingauge databased Bay of Bengal coastal rains over India seem to support the influence of aerosols on the precipitation. Further research with other ADE and AIE parameterizations is warranted and we encourage other modelers to pursue it utilizing aerosol models.

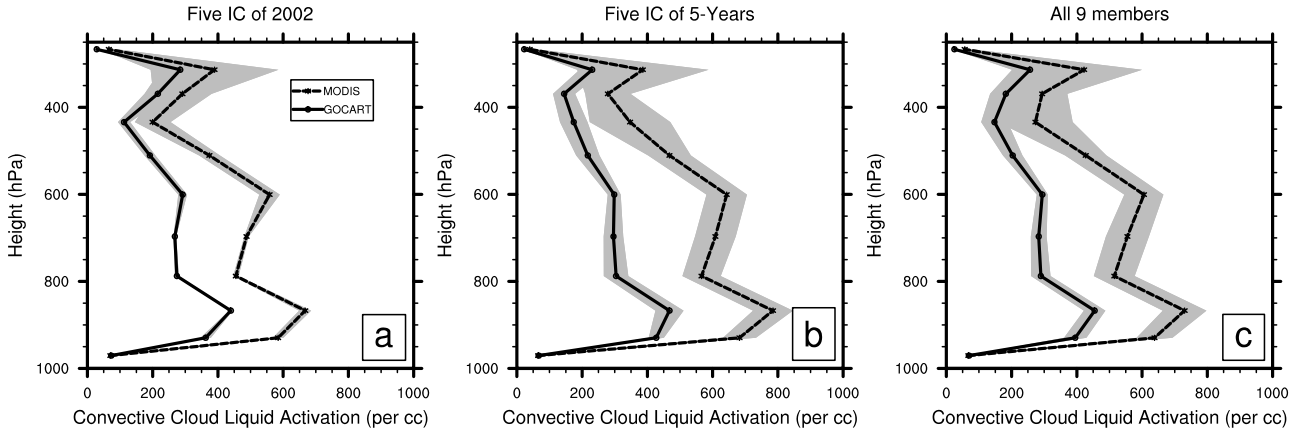

Figure 18. Liquid cloud activation nuclei per cubic centimeter over Arabian Sea from GOCART (climatology) and MODIS aerosol forcing for (a) all the five experiments during 2002, (b) for all the five experiments during 5 years, and (c) for all the nine member simulations during the 5 years. The shaded region on each curve shows the 95% confidence band for that ensemble calculated using a Student's *t* test.

[36] **Acknowledgment.** This work was supported by NSF grant ATM-0533966.

References

Adler, R. (2006), NASA Facts: TRMM Instruments, TRMM Microwave Imager, NASA-GSFC, 21 November. (Available at http://trmm.gsfc.nasa.gov/overview_dir/tmi.html)

Chin, M., P. Ginoux, S. Kinne, O. Torres, B. Holben, B. N. Duncan, R. V. Martin, J. A. Logan, A. Higurashi, and T. Nakajima (2002), Tropospheric aerosol optical thickness from the GOCART model and comparisons with satellite and Sun photometer measurements, *J. Atmos. Sci.*, *59*, 461–483.

Chou, M.-D., and M. J. Suarez (1994), An efficient thermal infrared radiation parameterization for use in general circulation models, *NASA Tech. Memo. 104606*, vol. 3, 85 pp. (NTIS N95-15745).

Chou, M. D., M. J. Suarez, C. H. Ho, M. M. H. Yan, and K. T. Lee (1998), Parameterizations for cloud overlapping and shortwave singlescattering properties for use in general circulation and cloud ensemble models, *J. Clim.*, *11*, 202–214.

Fountoukis, C., and A. Nenes (2005), Continued development of a cloud droplet formation parameterization for global climate models, *J. Geophys. Res.*, *110*, D11212, doi:10.1029/2004JD005591.

Gradel, T. E., and P. J. Crutzen (1993), *Atmospheric Change: An Earth System Perspective*, W. H. Freeman, New York.

Hubanks, P. (2007), Introduction to MODIS Atmosphere Level-2 Aerosol Products, NASA-GSFC, 6 June. (Available at http://modis-atmos.gsfc.nasa.gov/MOD04_L2/index.html)

Kaufman, Y. J., I. Koren, L. Remer, D. Rosenfeld, and Y. Rudich (2005), The effect of smoke, dust, and pollution aerosol on shallow cloud development over the Atlantic Ocean, *PNAS*, *102*(32), 11,207–11,212.

Khvorostyanov, V. I., and J. A. Curry (1999a), Toward the theory of stochastic condensation in clouds. part I: A general kinetic equation, *J. Atmos. Sci.*, *56*, 3985–3996.

Khvorostyanov, V. I., and J. A. Curry (1999b), Toward the theory of stochastic condensation in clouds. part II: Analytical solutions of the gamma-distribution type, *J. Atmos. Sci.*, *56*, 3997–4013.

Krishnamurti, T. N., B. Jha, P. J. Rasch, and V. Ramanathan (1997), A high resolution global reanalysis highlighting the winter monsoon. part I: Reanalysis fields, *Meteorol. Atmos. Phys.*, *64*, 123–150.

Lau, K.-M., and K.-M. Kim (2007), How nature foiled the 2006 hurricane forecasts, *Eos Trans. AGU*, *88*(9), doi:10.1029/2007EO090002.

Lau, K.-M., M. K. Kim, and K. M. Kim (2006), Asian summer monsoon anomalies induced by aerosol direct forcing: The role of the Tibetan plateau, *Clim. Dyn.*, *26*, 855–864, doi:10.1007/s00382-006-0114-z.

Lau, K. M., et al. (2008), The joint aerosol–monsoon experiment: A new challenge for monsoon climate research, *Bull. Am. Meteorol. Soc.*, *89*, 369–383.

Lelieveld, J., et al. (2001), The Indian Ocean experiment: Widespread air pollution from south and southeast Asia, *Science*, *291*(5506), 1031–1036.

Liu, X., and J. E. Penner (2005), Ice nucleation parameterization for global models, *Meteorol. Z.*, *14*(4), 499–514.

Lobert, J. M., and J. M. Harris (2002), Trace gases and air mass origin at Kaashidhoo, Indian Ocean, *J. Geophys. Res.*, *107*(D19), 8013, doi:10.1029/2001JD000731.

Lorentz, K. (2007), A-Train Constellation. NASA-GSFC, 14 June. (Available at http://www-calipso.larc.nasa.gov/about/atrain.php)

Menon, S., A. D. D. Genio, D. Koch, and G. Tselioudis (2002), GCM simulations of the aerosol indirect effect: Sensitivity to cloud parameterization and aerosol burden, *J. Atmos. Sci.*, *59*, 692–713.

Moorthi, S., and M. J. Suarez (1992), Relaxed Arakawa-Schubert: A parameterization of moist convection for general-circulation models, *Mon. Weather Rev.*, *120*, 978–1002.

Phadnis, M. J., H. Levy II, and W. J. Moxim (2002), On the evolution of pollution from south and southeast Asia during the winter-spring monsoon, *J. Geophys. Res.*, *107*(24), 4790, doi:10.1029/2002JD002190.

Platnick, S. K., M. D. Ackerman, S. A. Menzel, W. P. Baum, B. A. Riedi, J. C. Frey, and A. Richard (2003), The MODIS cloud products: Algorithms and examples from Terra, *IEEE Trans. Geophys. Remote Sensing*, *41*(2), 459–473, doi:10.1109/TGRS.2002.808301.

Ramanathan, V., and P. J. Crutzen (2003), New directions: Atmospheric brown clouds, *Atmos. Environ.*, *37*, 4033–4035.

Ramanathan, V., P. J. Crutzen, T. J. Kiehl, and D. Rosenfeld (2001a), Aerosols, climate and the hydrological cycle, *Science*, *294*, 2119–2124.

Ramanathan, V., et al. (2001b), The Indian Ocean experiment: An integrated analysis of the climate forcing and effects of the Great Indo-Asian haze, *J. Geophys. Res.*, *106*, 28,371–28,398.

Ramanathan, V., and M. V. Ramana (2005), Persistent, widespread, and strongly absorbing haze over the Himalayan foothills and the Indo-Gangetic plains, *Pure Appl. Geophys.*, *162*, 1609–1626.

Ramanathan, V., C. Chung, D. Kim, T. Bettge, L. Buja, J. T. Kiehl, W. M. Washington, Q. Fu, D. R. Sikka, and M. Wild (2005), Atmospheric brown clouds: Impacts on South Asian climate and hydrological cycle, *Proc. Natl. Acad. Sci. U.S.A.*, *102*, 5326–5333.

Reynolds, R. W., and T. M. Smith (1994), Improved global sea surface temperature analyses using optimum interpolation, *J. Clim.*, *7*, 929–948.

Satheesh, S. K., and V. Ramanathan (2000), Large difference in tropical aerosol forcing at the top of the atmosphere and Earth's surface, *Nature*, *405*, 60–63.

Satheesh, S. K., V. Ramanathan, B. N. Holben, K. K. Moorthy, N. G. Loeb, H. Maring, J. M. Prospero, and D. Savoie (2002), Chemical, microphysical, and radiative effects of Indian Ocean aerosols, *J. Geophys. Res.*, *107*(D23), 4725, doi:10.1029/2002JD002463.

Seifert, A., and K. D. Beheng (2001), A double-moment parameterization for simulating autoconversion, accretion and self collection, *Atmos. Res.*, *59*, 265–281.

Simpson, J., R. F. Adler, and G. R. North (1988), A proposed tropical rainfall measuring mission (TRMM) satellite, *Bull. Am. Meteorol. Soc.*, *69*, 278–295.

Sud, Y. C., and D. Lee (2007), Parameterization of aerosol indirect effect to complement McRAS cloud scheme and its evaluation with the 3-year ARM-SGP analyzed data for single column models, *Atmos. Res.*, *86*, 105–125.

Sud, Y. C., and G. K. Walker (1999a), Microphysics of clouds with the relaxed Arakawa-Schubert scheme (McRAS). part I: Design and evaluation with GATE phase III data, *J. Atmos. Sci.*, *56*, 3196–3220.

Sud, Y. C., and G. K. Walker (1999b), Microphysics of clouds with the relaxed Arakawa-Schubert scheme (McRAS). part II: Implementation and performance in GEOS II GCM, *J. Atmos. Sci.*, *56*, 3221–3240.

Sud, Y. C., and G. K. Walker (2003a), New upgrades to the microphysics and thermodynamics of clouds in McRAS: SCM and GCM evaluation of simulation biases in GEOS GCM, *Proc. Indian Natl. Sci. Acad.*, *69*(5), 543–565.

Sud, Y. C., and G. K. Walker (2003b), Influence of ice-phase physics of hydrometeors on moist-convection, *Geophys. Res. Lett.*, *30*(14), 1758, doi:10.1029/2003GL017587.

Takemura, T., Y. Kaufman, L. A. Remer, and T. Nakajima (2007), Two competing pathways of aerosol effects on cloud and precipitation formation, *Geophys. Res. Lett.*, *34*, L04802, doi:10.1029/2006GL028349.

A. Chakraborty, T. N. Krishnamurti, and A. Martin, Department of Meteorology, Florida State University, Room 404 Love Building, 1017 Academic Way, Tallahassee, FL 32306-4520, USA. (tnk@io.met.fsu.edu)

K.-M. Kim, Y. Sud, and G. Walker, Climate and Radiation Branch-Code 613.2, NASA Goddard Space Flight Center, Greenbelt, MD 20771, USA.

W. K. Lau, The Laboratory for Atmospheres-Code 613, NASA Goddard Space Flight Center, Greenbelt, MD 20771, USA.